Distribution Agreement

In presenting this thesis or dissertation as a partial fulfillment of the requirements for an advanced degree from Emory University, I hereby grant to Emory University and its agents the non-exclusive license to archive, make accessible, and display my thesis or dissertation in whole or in part in all forms of media, now or hereafter known, including display on the world wide web. I understand that I may select some access restrictions as part of the online submission of this thesis or dissertation. I retain all ownership rights to the copyright of the thesis or dissertation. I also retain the right to use in future works (such as articles or books) all or part of this thesis or dissertation.

Signature:

_____ _____

Jennifer R. Merritt Date

A supergene-linked estrogen receptor drives alternative phenotypes in a polymorphic songbird

By

Jennifer R. Merritt

Doctor of Philosophy
Psychology

_____
Donna L. Maney
Advisor

_____
Patricia A. Brennan
Committee Member

_____
Eric A. Ortlund
Committee Member

_____
Kim Wallen
Committee Member

_____
Soojin V. Yi
Committee Member

Accepted:

_____
Lisa A. Tedesco, Ph.D.
Dean of the James T. Laney School of Graduate Studies

_____
Date

A supergene-linked estrogen receptor drives alternative behavioral phenotypes in a polymorphic songbird

By

Jennifer R. Merritt
M.A., Emory University, 2016
B.A., University of Illinois at Urbana-Champaign, 2013

Advisor: Donna L. Maney, Ph.D.

An abstract of
a dissertation submitted to the Faculty of the
James T. Laney School of Graduate Studies of Emory University
in partial fulfillment of the requirements for the degree of
Doctor of Philosophy
in Psychology
2020

Abstract

A supergene-linked estrogen receptor drives alternative phenotypes in a polymorphic songbird

By Jennifer R. Merritt

Behavioral evolution relies on genetic changes, yet few behaviors can be traced to specific genetic sequences in vertebrates. Here, we show experimental evidence that differentiation of a single gene has contributed to the evolution of divergent behavioral phenotypes in the white-throated sparrow, a common backyard songbird. In this species, a series of chromosomal inversions has formed a supergene that segregates with an aggressive phenotype. The supergene has captured *ESR1*, the gene that encodes estrogen receptor α (ERα); as a result, this gene is accumulating changes that now distinguish the supergene allele from the standard allele. Our results show that in birds of the more aggressive phenotype, ERα knockdown caused a phenotypic change to that of the less aggressive phenotype. Next, we showed that in a free-living population, aggression is predicted by allelic imbalance favoring the supergene allele. Finally, we identified *cis*-regulatory features, both genetic and epigenetic, that explain the allelic imbalance. This work provides a rare illustration of how genotypic divergence has led to behavioral phenotypic divergence in a vertebrate.

A supergene-linked estrogen receptor drives alternative phenotypes in a polymorphic songbird

By

Jennifer R. Merritt
M.A., Emory University, 2016
B.A., University of Illinois at Urbana-Champaign, 2013

Advisor: Donna L. Maney, Ph.D.

A dissertation submitted to the Faculty of the
James T. Laney School of Graduate Studies of Emory University
in partial fulfillment of the requirements for the degree of
Doctor of Philosophy
in Psychology
2020

For Toni & Ken Merritt

Acknowledgments

First and foremost, I would like to thank my advisor Dr. Donna Maney for six years of mentorship and dedication to my training. I also want to thank my thesis committee members Drs. Patricia Brennan, Eric Ortlund, Kim Wallen, and Soojin Yi for welcoming me into your labs, holding me to the highest standards, providing unflappable support, and offering guidance the whole way. Thank you to the faculty and students of NAB that shaped me into the scientist that I am today, and to the Psychology Department that made Emory feel like home.

I am extremely grateful to my colleagues in the Maney "Bird Brain" Lab who accompanied me through graduate school. I don't have enough space here to thank Drs. Kathleen Grogan, Nicole Baran, and Wendy Zinzow-Kramer for the endless advice, support, and inspiration. To my labmates Isabel Fraccaroli, Erik Iverson, T.J. Libecap, Natalie Pilgeram, Kenzie Prichard, and Dr. Carlos Rodriguez-Saltos, thanks for the solidarity and laughter. In addition to those mentioned above, thank you to the incredibly smart and talented undergraduates and high school students that made my research a reality: Matthew Davis, George Jiang, Emily Kim, Abhinav Nair, Kennedy Richardson, and Donny Williams. In addition, I thank Hyeonsoo "Harris" Jeong, Dr. Aubrey Kelly, Dr. Suzanne Mays, Carmen Shaw, and Dr. Dan Sun for your insight and training. And finally, none of this would have been possible without my undergraduate mentors at the University of Illinois at Urbana-Champaign, Drs. Justin Rhodes and Janice Juraska, who offered me the opportunities to turn a love of science into a career and encouraged me to go to graduate school.

Many thanks to the staff that make the science possible, including Kate Coblin, Lorenza Houser, Paula Mitchell, Emily Stills, and Tonya Woolcock for their help over the years. To the fantastic staff at the Rollins Café, Pam Andrews and Ronnie Byrd, thank you for keeping me caffeinated, sane, and fed. Thank you to the countless staff at the O. Wayne Rollins Research Center that made our lab a comfortable, functional work space and to those that cared about the well-being of my animals as much as I did, especially Keith Worthy and André Abraham.

Finally, thank you to the friends and family (immediate and extended) that cheered me on, conspired with me, and showed me compassion even as I missed holidays, birthdays, engagements, babies, degrees, and promotions. I could not have done this without you. Thank you to Dr. Amy Goch who made me unrecognizably more capable. To my grad school friends: navigating grad school with you was a blast; I cannot wait to debate, celebrate, and explore with you to infinity and beyond. To my life-long friends near and far, thank you always supporting me. Endless thanks to my parents, Ken and Liz Merritt, for your love and for always encouraging me to discover the answers to my own questions. To my sisters Emily, Grace, and Sara, and my niece Alana, your encouragement was invaluable. Thank you to my grandfather Ken Merritt for displaying a life-long love of learning. Lastly, to my role model, my grandma Toni Merritt (1944-2020), who encouraged me by demonstrating what it means to be an independent, educated woman who perseveres against all odds.

Table of Contents

List of Tables

List of Figures

List of Symbols and Abbreviations

6-FAM	6-carboxyfluorescein
AI	allelic imbalance
AIC	Akaike information criterion
AP	anterior-posterior axis
bsDNA	bisulfite-converted DNA
cDNA	complementary DNA
CON	control
Cp	crossing point
CpG	cytosine and guanine bases connected by a phosphate group
CRE	*cis*-regulatory element
Cy5	cyanine
DMEM	Dulbecco's Modified Eagle Medium
DNA	deoxyribonucleic acid
DV	dorsal-ventral axis
E2	17β-estradiol
ERα	estrogen receptor alpha, protein symbol
ESR1	estrogen receptor alpha, gene symbol
ESR1-KD	estrogen receptor alpha knockdown
ESR2	estrogen receptor beta, gene symbol
gDNA	genomic DNA
FBS	fetal bovine serum
FDR	false discovery rate

GAPDH	glyceraldehyde-3-phosphate dehydrogenase, gene symbol
GLM	generalized linear model
GRM1	glutamate metabotropic receptor 1, gene symbol
HEK 293	Human embryonic kidney 293 cells
HYP	hypothalamus
LNA	locked nuclei acid
LUC	luciferase, gene symbol
MEMα	Minimum Essential Medium, no nucleosides
$MgCl_2$	magnesium chloride
mGluR	glutamate metabotropic receptor 1, protein symbol
ML	medial-lateral axis
NCOA7	nuclear receptor coactivator 7, gene symbol
ns	not significant
PE	paired-end
PPIA	peptidylprolyl isomerase A, gene symbol
qPCR	quantitative polymerase chain reaction
RLU	relative light units
RNA	ribonucleic acid
rPOM	rostral portion of the medial preoptic area
SNP	single nucleotide polymorphism
STI	simulated territorial intrusion
SV40	simian vacuolating virus
VIP	vasoactive intestinal peptide, gene symbol

TBP	TATA box binding protein, gene symbol
TF	transcription factor
TnA	nucleus taeniae of the amygdala
TS	tan-striped
WS	white-striped
ZAL	*Zonotrichia albicollis*

Introduction

There is no doubt that many social behaviors have a genetic basis. They are heritable, acted on by natural selection, and they evolve (Wilson, 2000). Nevertheless, few genetic sequences have been directly linked to social behaviors in vertebrates. Most behavioral phenotypes are polygenic, and social behavior itself is flexibly expressed depending on context. This complexity, together with the many levels of biological organization separating a gene sequence from a social behavior, has made it difficult to completely understand why and how natural genotypic variation contributes to behavioral phenotypes (Bendesky & Bargmann, 2011; Merritt, 2019; Niepoth & Bendesky, 2020; Robinson, Grozinger, & Whitfield, 2005; Snyder-Mackler & Tung, 2017).

The most promising animal models for identifying genetic targets of behavioral evolution are those with well-documented genetic variation linked to clear behavioral phenotypes. To date, these organisms include *Microtus* voles (Madrid, Parker, & Ophir, 2020) and *Peromyscus* mice (Bendesky et al., 2017), in which genetic variation in the vasopressin system has been causally linked with variation in affiliative and parental behavior, respectively. Other promising models include organisms in which a behavioral phenotype is linked with large-scale changes in genomic architecture. In fire ants (*Solenopsis invicta*), for example, the social structure of colonies segregates with a chromosomal inversion inside which recombination is suppressed, leading to the formation of a 'supergene', or a group of genes that are 'locked' together through linkage disequilibrium and inherited as a unit (Wang et al., 2013). Similarly, in ruffs (*Philomachus pugnax*), a chromosomal inversion appears to mediate a number of alternative reproductive strategies (Kupper et al., 2016; Lamichhaney et al., 2016),

although the causal genes have not been identified.

Decades before the discovery of the chromosomal inversions in fire ants and ruffs, Thorneycroft (Thorneycroft, 1966, 1975) described a rearrangement of the second chromosome in white-throated sparrows (*Zonotrichia albicollis*), a common North American songbird. This rearrangement, which has been called ZAL2^{m} ('m' for metacentric) segregates with a plumage morph. WS birds of both sexes possess a copy of ZAL2^{m}, whereas birds of the TS morph are homozygous for the standard arrangement, ZAL2 (Fig. 1A) (Thomas et al., 2008). The rearrangement is maintained in the population because of the species' unique disassortative mating system; nearly every breeding pair consists of one individual of each morph (Tuttle et al., 2016). Because almost all WS birds are heterozygous for ZAL2^{m} (Horton et al., 2013; Tuttle et al., 2016), this mating

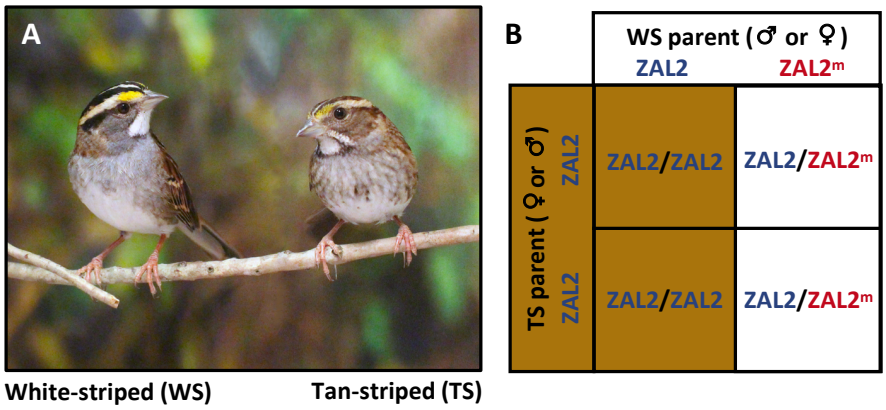

Figure 1. Polymorphism in white-throated sparrows. (A) White-throated sparrows occur in two morphs: a more aggressive WS morph and a less aggressive TS morph. WS birds are heterozygous for a rearrangement of chromosome 2, known as ZAL2^{m}, which functions as a supergene. Note that we follow conventional nomenclature for avian chromosomes, numbering them from largest to smallest (Ladjali-Mohammedi, Bitgood, Tixier-Boichard, & De Leon, 1999). Chromosome 2 in white-throated sparrows corresponds to chromosome 3 in chickens (Thomas et al., 2008). (B) Nearly all breeding pairs consist of one TS (ZAL2/ZAL2) bird and one WS (ZAL2/ZAL2^{m}) bird. As a result, approximately 50% of the offspring are ZAL2/ZAL2^{m} heterozygotes and thus WS, and the rest are ZAL2/ZAL2 homozygotes and thus TS. Photo courtesy of Jennifer Merritt.

system keeps ZAL2^{m} in a near-constant state of heterozygosity (Fig. 1B), profoundly suppressing recombination and causing it to differentiate from ZAL2 (Davis et al., 2011; Tuttle et al., 2016).

The rearranged region of ZAL2^{m} in white-throated sparrows can be regarded as a supergene because it harbors a discrete set of co-inherited, co-evolving genes that influence a suite of traits; the supergene dictates not only plumage coloration, but also levels of territorial aggression. In both field and laboratory studies, WS birds have been shown to be more aggressive than TS birds. In free-living, breeding populations, for example, WS birds of both sexes respond to STI with higher levels of aggression than do their TS counterparts (Falls & Kopachena, 2020; Horton, Moore, & Maney, 2014). ZAL2^{m}/ZAL2^{m} homozygotes are quite rare (Romanov, Dodgson, Gonser, & Tuttle, 2011; Tuttle et al., 2016); those that have been described were extraordinarily aggressive (Falls & Kopachena, 2020; Horton et al., 2013). Thus, the ZAL2^{m} rearrangement is associated with aggression in a dose-dependent manner.

Territorial aggression in songbirds has been strongly linked to circulating levels of gonadal steroid hormones (Ketterson & Nolan, 1992; Wingfield, Hegner, Dufty, & Ball, 1990). In white-throated sparrows, WS birds have higher plasma testosterone and E2 than TS birds (Horton, Moore, et al., 2014); this difference does not, however, explain the morph difference in aggression. Even when plasma testosterone or E2 is experimentally equalized, WS birds are still more aggressive (Maney, Lange, Raees, Reid, & Sanford, 2009; Merritt et al., 2018). This finding suggests that WS birds are more sensitive than TS birds to the behavioral effects of these hormones, perhaps because of differential expression of a steroid hormone receptor. One of the genes inside the

supergene is *ESR1* (Thomas et al., 2008) which encodes estrogen receptor α (ERα). In rodents, manipulation of *ESR1* expression increases aggressive behavior and inhibits prosocial behavior (Ogawa, Lubahn, Korach, & Pfaff, 1997; Stetzik et al., 2018; Trainor, Kyomen, & Marler, 2006). In songbirds, including white-throated sparrows, *ESR1* expression in some brain regions is predictive of territorial aggression (Horton, Hudson, et al., 2014; Rosvall et al., 2012). Thus, it is particularly compelling that this gene is locked inside the ZAL2/2^{m} rearrangement.

ESR1 resides entirely within the rearrangement (Thomas et al., 2008) and has accumulated nucleotide divergence between the ZAL2 and ZAL2^{m} alleles. The resulting fixed non-synonymous mutations are not likely to affect receptor function, however. Instead, variation in regulatory regions has been introduced that could alter levels of expression (Horton, Hudson, et al., 2014). The following observations suggest that the genetic differentiation between the ZAL2 and ZAL2^{m} alleles of *ESR1* could explain the behavioral polymorphism in this species. First, *ESR1* is differentially expressed between the morphs in several brain regions associated with social behavior (Horton, Hudson, et al., 2014). Second, expression in some of these regions predicts aggressive behavior better than does morph (Horton, Hudson, et al., 2014). Third, exogenous E2 facilitates aggression in WS but not TS birds (Maney et al., 2009; Merritt et al., 2018). Thus, we hypothesized that *cis*-regulatory variation in *ESR1* leads to differential expression between the morphs, and that differential expression of *ESR1* causes the aggressive phenotype. Support for these hypotheses would allow us to causally connect genotype to phenotype.

Materials and Methods

All procedures involving animals were approved by the Emory University Institutional Animal Care and Use Committee, were in keeping with all federal, state, and local laws, and adhered to guidelines set forth by the National Institutes of Health Guide for the Care and Use of Laboratory Animals. All data were analyzed in RStudio (v1.2.1335; R v3.6.0). The α level was set at $p \leq 0.05$ unless otherwise specified. More detailed information is provided in the Appendix.

Effects of *ESR1* knockdown on aggression

Animals. We collected 33 white-throated sparrows on the campus of Emory University in Atlanta, GA during fall migration, when gonads are regressed and plasma levels of sex steroids are low. We maintained the birds in a nonbreeding state by housing them under short day lengths (10-h light:14-h dark) (Maney, 2008; Matragrano, LeBlanc, Chitrapu, Blanton, & Maney, 2013). Our rationale for testing birds in non-breeding condition was that (1) the morph difference in *ESR1* expression in TnA is pronounced in non-breeding birds (Maney, Horton, & Zinzow-Kramer, 2015) and (2) ERα would be relatively unoccupied and thus manipulatable with exogenous E2 (Merritt et al., 2018). Each bird was fitted with bilateral 26-gauge, stainless steel guide cannulae aimed at TnA (AP 0.0 mm, ML 1.9 mm, DV -3.6 mm). Birds recovered from surgery for at least 3 days before dominance testing. After recovery, dominance relationships between pairs of birds were established following (Merritt et al., 2018). Dyads were comprised of a dominant bird, which was used as the focal animal, and a subordinate opponent.

Antisense. *ESR1* expression was manipulated with custom-designed LNA 15-mer antisense oligonucleotides, avoiding ZAL2/ZAL2^{m} SNPs (*ESR1*-KD; TTCAAAGGTGGCACT). A scrambled control oligonucleotide was designed to consist of the same nucleotides but in a random order (TAGCATGTCAGATCG). Both the *ESR1*-KD and scrambled sequences were entered into BLAST (NCBI) and *Zonotrichia albicollis* refseq_rna was searched to confirm no significant alignments to other transcripts, in particular *ESR2* (XM_014270428.2). Starting on the day after the establishment of a dyad, we made a series of four infusions of antisense or scrambled oligos, 2 per day.

Behavioral testing. Behavioral testing was conducted, as previously described (Merritt et al., 2018), the day after the fourth infusion. In brief, before a behavioral trial, we placed the focal bird in its cage in an empty sound-attenuating booth to acclimate it to that environment. After 1 h, we placed the opponent in its cage immediately adjacent to the focal bird's cage with an opaque barrier between the cages that visually isolated the birds from each other. At the same time, a wax moth larva that had just been injected with 300 µg of cyclodextrin-encapsulated E2 or cyclodextrin alone (CON) was placed on the floor of the focal bird's cage. This oral dosage of E2 increases plasma E2 to a similar extent in WS and TS birds, and produces levels typical of breeding WS females within 15 min (Merritt et al., 2018). Ten min after the focal bird consumed the larva, the opaque barrier was removed and the birds were allowed to interact for 10 min. Videos of the trials were later scored for attacks directed toward the opponent and time spent in proximity to the opponent. After a washout period of 48 hours, each focal bird participated in a second trial with the other hormone treatment (CON or E2). All trials

were counterbalanced with respect to the order of treatment. On the day after the second behavioral trial, brains were harvested and each cannula was injected with bromophenol blue to confirm its placement. Levels of *ESR1* and *ESR2* expression were measured in samples of TnA using qPCR (Table A1). The final sample size for each group, each of which included multiple males and females, was n = 6 for WS *ESR1*-KD, n = 7 for WS scrambled, n = 6 for TS *ESR1*-KD, and n = 7 for TS scrambled. We used separate GLMs to test whether the effect of hormone treatment depended on morph separately in birds receiving scrambled or *ESR1*-KD oligonucleotides, as well as whether the effect of hormone treatment depended on antisense in TS or WS birds (Table A2). We then followed up significant 2-way interactions by testing for the effect of treatment within each experimental group (WS *ESR1*-KD, WS scrambled, TS *ESR1*-KD, TS scrambled; Table A3).

Quantification of *ESR1* allelic imbalance

Animals. Adults and nestlings of both sexes were collected during the breeding season at Penobscot Experimental Forest near Argyle, ME. Adults were collected during the peak of territorial behavior, after pair formation and territory establishment but before or early in the incubation stage (Falls & Kopachena, 2020; Horton, Moore, et al., 2014; Zinzow-Kramer et al., 2015). Before collecting the adults, we characterized their behavioral responses to territorial intrusion by conducting STIs (Horton, Hauber, & Maney, 2012). Birds remained on their territories for at least 24 hrs before we returned to collect tissue, in order to minimize the effects of the STI itself on gene expression. Later, during the parental phase of the breeding season, we collected nestlings on post-hatch day

seven, two days before natural fledging (Horton, Moore, et al., 2014; Huynh, Maney, & Thomas, 2011). All brains were rapidly dissected from the skulls, frozen on dry ice and stored at -80 °C. RNA and DNA were extracted from samples of TnA, HYP, and rPOM, and RNA was reverse-transcribed into cDNA for the allelic imbalance assay (Grogan, Horton, Hu, & Maney, 2019; Zinzow-Kramer et al., 2015).

Allelic imbalance assay. Allelic imbalance was assessed using a multiplexed qPCR assay with probes specific for each allele of *ESR1*. Primers and probes were designed by Integrated DNA Technologies to target a SNP within *ESR1* Exon 1A. Only WS birds were used in these assays because TS birds do not have the ZAL2^{m} allele. We calculated the relative expression of each allele within each reaction and then averaged across three replicate reactions. The ratio for each cDNA sample was then normalized to the average of the ratios calculated from WS gDNA samples (mean, 0.99, minimum, 0.95, maximum, 1.02) to correct for the relative affinity of each probe to its target sequence. We tested for allelic imbalance within each region and age using one-sample t-tests, comparing the allelic ratios with a null ratio of 1 (Table A4). To determine whether the degree of imbalance varied by age or region, we analyzed the data in a two-way mixed ANOVA with region and age as factors (Table A5), followed by Tukey's Honest Significant Difference test (Table A6). Associations between allelic imbalance and territorial responses were tested using Pearson's correlations.

Analysis of *cis*-regulatory variation in *ESR1*

Analysis of transcription factor binding sites. We examined the CREs in *ESR1* to identify transcription factor binding sites that are disrupted by ZAL2/2^{m} (Table A6). To predict differential transcription factor binding between the two alleles, we used sTRAP (Manke, Heinig, & Vingron, 2010; Okhovat, Maguire, & Phelps, 2017), a tool that predicts the binding affinities of transcription factors to each allele and ranks them according to the extent to which the variation affects their binding affinity. We then cross-referenced the list of factors predicted to bind differentially to the two alleles with the list of factors that are expressed in TnA using our RNA-seq data (Zinzow-Kramer et al., 2015).

Luciferase assays. We cloned each allele of the 2-kb CREs A, B, and C into the pGL3-control vector upstream of *LUC*. Constructs were co-transfected with *Renilla* luciferase into cultured cells. At 24 h after transfection, luciferase activity was quantified using the Promega Dual-Glo assay system on a Biotek Synergy plate reader. The value for the ZAL2^{m} allele was normalized to the value for the ZAL2 allele, meaning that the ZAL2^{m} data were expressed relative to a value of 1 for the ZAL2 allele. Effects of CRE, allele, and interactions between CRE and allele were assessed using 2-way ANOVA followed by Student's pairwise t-tests (Table A7).

Analysis of DNA methylation. We bisulfite-converted gDNA extracted from samples of TnA from the behaviorally characterized, free-living adults described above. Amplicons containing shared and unshared CpG sites in the three CREs and exon 1A of *ESR1* (Table A8) were amplified using PCR with primers not falling on SNPs or CpGs

(Table A9). Amplicons were pooled per sample, indexed, then pooled for a single sequencing run (PE300) on an Illumina MiSeq system. Reads were filtered, trimmed and aligned to a bisulfite-converted, N-masked reference genome, and then assigned to an allele (Sun et al., 2020). Allele-specific methylation was determined by Bismark (Krueger & Andrews, 2011). To arrive at an overall level of methylation for each of the two alleles for each bird, we averaged the percent methylation across all of the CpGs in that allele (Table A10). When including unshared CpG sites, we treated that site on the other allele as 0 percent methylation. Effects of allele and CRE were tested using linear mixed models, followed by contrasts of estimated marginal means for shared sites only as well as for all possible CpG sites.

Results

ESR1 mediates an aggressive phenotype

ESR1 expression is several fold higher in WS than TS birds in nucleus taeniae of the amygdala (TnA) (Grogan et al., 2019; Horton, Hudson, et al., 2014), also called the ventrolateral arcopallium (Mello, Kaser, Buckner, Wirthlin, & Lovell, 2019), which shares molecular markers, connectivity, and function with the medial amygdala of mammals (Cheng, Chaiken, Zuo, & Miller, 1999; Mello et al., 2019; Reiner et al., 2004). In this region, expression of *ESR1* predicts territorial aggression (Horton, Hudson, et al., 2014). We therefore hypothesized that this morph difference in *ESR1* expression contributes to the behavioral phenotype. To test this hypothesis, we built on our previous finding that a bolus dose of E2 enhances aggression, compared with vehicle, in WS but

not TS birds (Merritt et al., 2018). In other words, we knew that WS but not TS birds are sensitive to the effects of E2 on aggression (see also (Maney et al., 2009)). To test whether this morph-specific sensitivity can be explained by the morph difference in *ESR1* expression in TnA, we knocked down *ESR1* expression in TnA using antisense oligonucleotides (Fig. 2A; Table A1). Our rationale for this approach was the following: if we knocked down *ESR1* expression in TnA to a TS-like level in WS birds, then the behavioral response to E2 in those WS birds would be TS-like (low response) and the morph difference in aggression would be abolished.

This prediction was supported by our findings. In animals treated with scrambled (CON) oligonucleotides, an oral bolus dose of E2 enhanced aggression toward a same-morph conspecific (Fig. 2B, C, F). This effect was observed in WS birds but not in TS birds (morph × treatment interaction, $P < 0.01$, Table A2), consistent with previous findings (Maney et al., 2009; Merritt et al., 2018). In other words, the morph with naturally higher expression of *ESR1* in TnA responded to exogenous E2 but the morph with low expression did not. When the morph difference in *ESR1* expression in TnA was then abolished via administration of antisense oligonucleotides (Fig. 2A), E2-induced aggression in WS birds was indistinguishable from that in TS birds (Fig. 2C, F). Thus, WS-typical levels of *ESR1* expression in TnA were necessary for E2 to facilitate aggression (see also Tables A1 to A3).

To provide further support for the explanatory power of *ESR1*, we next tested for a correlation between the aggressive behavior in the behavioral trials described above (Fig. 2B) and the level of *ESR1* expression in TnA. At 24 h after the second behavioral trial, brains were collected and mRNA extracted from TnA in each bird. Even when our

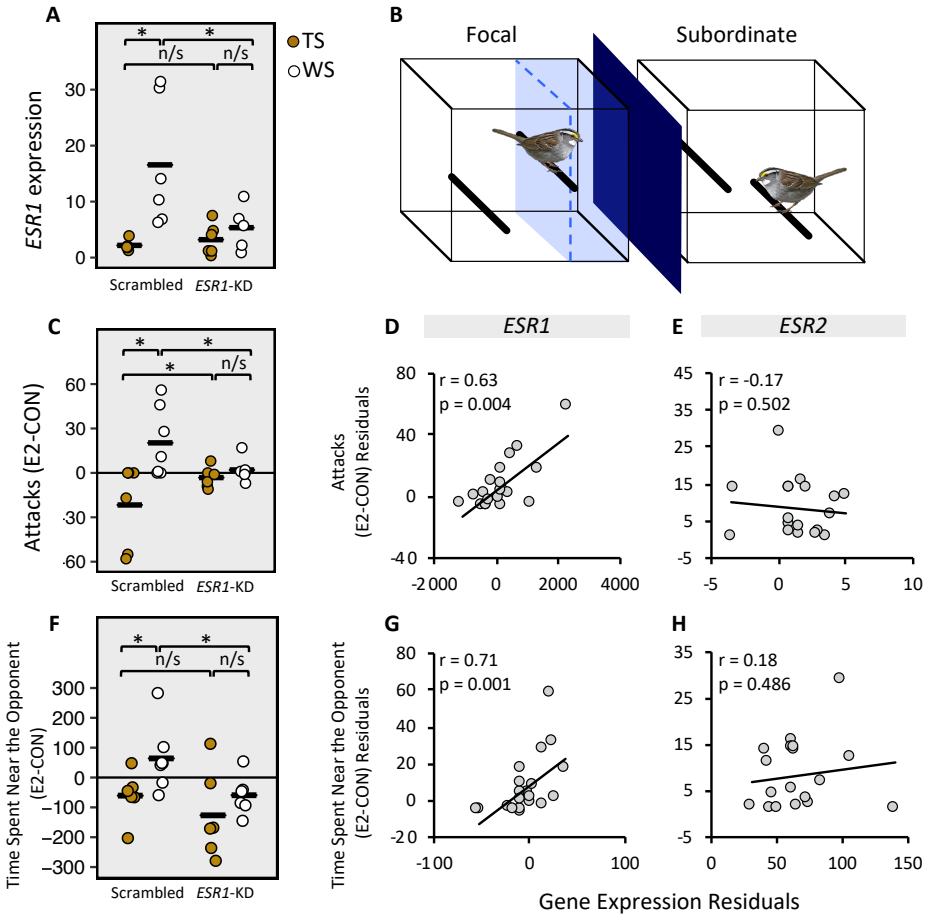

Figure 2. *ESR1* expression mediates the morph difference in aggression. (A) *ESR1* expression was reduced by *ESR1*-KD in TnA. Data are shown for pooled left and right TnA for each animal. Horizontal bars represent means (n = 6 or 7 per group). (B) During behavioral testing, the cages of the focal bird and a subordinate were separated by a visual barrier (dark blue; cage and bird not drawn to scale). Ten min after oral administration of E2 or CON, the visual barrier was removed for 10 min. Reprinted from Merritt et al., Copyright (2018), with permission from Elsevier. (C-H) the Y-axes depict the changes in behavior between the CON and E2 trials. *ESR1* knockdown significantly reduced the degree to which E2 increased the number of attacks (C) and the time spent near the opponent (in the light blue area in B) in WS birds only (F). Both behaviors were correlated with the level of *ESR1* expression (D and G) but not with the level of *ESR2* expression (E and H) (n = 20). Residuals from a partial correlation controlling for morph are plotted in D, E, G, and H. Only birds receiving infusions of scrambled oligonucleotides (n=13) and birds in which the cannulae missed TnA (n = 7) were included in analyses of *ESR1* and *ESR2* expression. All birds were laboratory-housed. More information is provided in Tables 1 to 3. * $P < 0.05$, horizontal bars represent means.

analysis was limited to the control animals and "misses", in other words animals not receiving knockdown in TnA (total n = 20), *ESR1* expression in TnA predicted aggression independently of morph (Fig. 2D,G). *ESR2,* a paralog of *ESR1* that is not differentially expressed by morph and is not on chromosome 2 (Zinzow-Kramer et al., 2015), did not predict aggression (Fig. 2E,H) or *ESR1* expression (Fig. A1). These results, from laboratory-housed birds, replicate our findings in free-living populations (Horton, Hudson, et al., 2014) that *ESR1* expression, in TnA specifically, predicts aggressive behaviors.

Allelic imbalance in *ESR1* expression

We showed above that the aggressive phenotype of WS birds is mediated by their increased *ESR1* expression in TnA, compared with TS birds. We next hypothesized that this differential expression, which leads to differential behavior, is mediated by divergence of *cis*-regulatory regions of the *ESR1* gene. To test for differential regulation of the *ESR1* alleles, we quantified the AI, in other words the degree to which one allele is expressed more than the other, in TnA (Fig. 3). We conducted this study using tissue from free-living WS birds ($ZAL2^m$/ZAL2 heterozygotes) in breeding condition, collected from our field site near Argyle, Maine. We quantified aggressive responses to an STI, during which a caged male decoy was placed onto a resident pair's territory, conspecific male song was played through a speaker, and the aggressive responses of the residents were observed for 10 min (Horton, Moore, et al., 2014). Because *ESR1* expression in TnA is strongly correlated with the amount of singing in response to STI (Horton, Hudson, et al., 2014), we focused on

that behavior in particular. Tissue was collected 24 h later to minimize the effect of the STI itself on gene expression, and allelic imbalance was measured via qPCR. In the same birds, we looked for allelic imbalance in two other regions of the brain: rPOM and HYP. Levels of *ESR1* expression differ between the morphs in these regions, albeit to a much lesser extent than in TnA (Grogan et al., 2019; Horton, Hudson, et al., 2014).

We detected allelic imbalance in all three brain regions. The ZAL2 allele was overexpressed, relative to the ZAL2^{m} allele, in HYP and rPOM (Fig. 3A,D and Tables A4

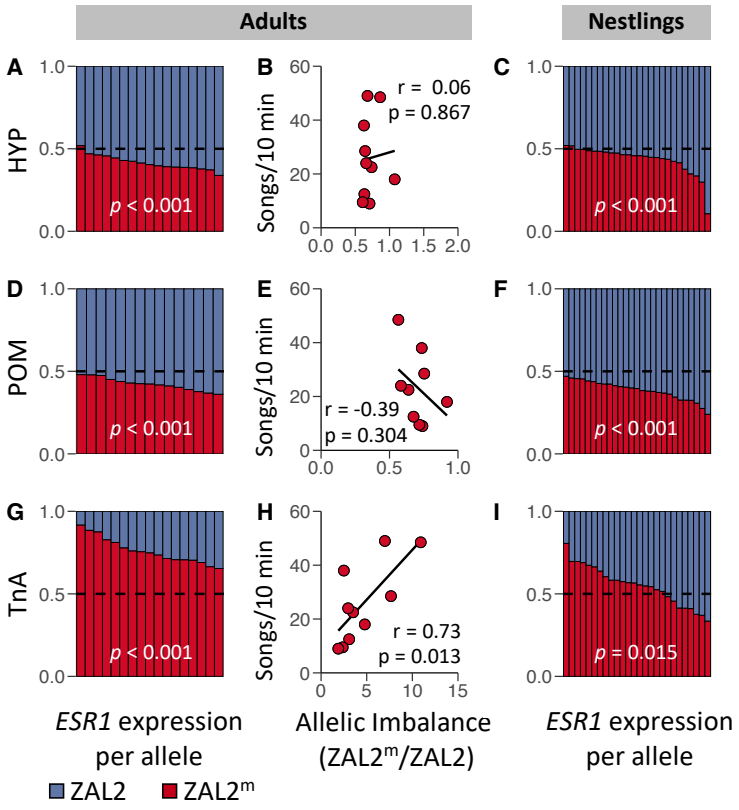

Figure 3. AI in *ESR1* expression. We quantified AI in three brain regions in heterozygous (WS) adults (A, D, and G) and nestlings (C, F, and I) sampled from a free-living population (adults n = 15 to18, nestlings n = 26 to 27). In the bar graphs, each column represents the relative expression of ZAL2 (blue) and ZAL2^{m} (red) in a single bird. The dashed line represents a null ratio of 0.5. Behavioral responses of adult males to STI (Methods) were not predicted by the degree of AI in HYP (B) or POM (E); however, they were significantly correlated with AI in TnA (H) (n =10). See Tables 4 and 5.

and A5); in contrast, the ZAL2^{m} allele was more highly expressed than ZAL2 in TnA (Fig. 3G). This imbalance predicted the territorial response to STI (Fig. 3H). In contrast, allelic imbalance in the HYP and rPOM did not predict that response (Fig. 3B and E). Thus, the degree to which a bird engaged in territorial aggression, which was markedly higher in the WS birds than in the TS birds (Horton, Hudson, et al., 2014; Horton, Moore, et al., 2014; Merritt et al., 2018), was predicted by the relative expression of the ZAL2^{m} allele.

Engaging in territorial aggression can affect plasma levels of steroid hormones (Wingfield et al., 1990) and presumably expression of steroid-related genes. Thus, it is possible that the correlation between aggressive behavior and *ESR1* allelic imbalance is caused by an effect of the behavior on expression. Therefore, we tested whether the pattern of allelic imbalance in adulthood is already present early in development, before birds are engaging in territorial aggression. Allelic imbalance was detected in nestlings in all three regions (all $P < 0.02$; Fig. 3C,F,I; Tables A4,5), and as was the case in adults, the ZAL2^{m} allele was expressed more than ZAL2 in TnA only (Fig. 3I). Overall expression of *ESR1* in TnA was higher in WS than TS nestlings at the same age (Grogan et al., 2019), showing that the pattern of AI and the morph difference in *ESR1* expression emerge early in development and are thus unlikely to be caused by engaging in territorial behavior.

Cis-regulation of *ESR1* expression

We showed above that *ESR1* expression in TnA is causal for an aggressive phenotype in WS birds, and that this aggressive phenotype is predicted by expression of the ZAL2^{m} allele specifically. We next explored the genetic and epigenetic mechanisms

underlying allelic imbalance. First, we hypothesized that *cis*-regulatory divergence has led to differential transcriptional activity of the two alleles, potentially because of divergence of transcription factor binding sites. Second, we hypothesized that epigenetic regulation of the *ESR1* promoter regions differs between the alleles, resulting in differential expression. In this species, *ESR1* contains three transcription start sites, which are used in the brain in both morphs (Fig. 4A) (Horton, Hudson, et al., 2014). The 2kb regions immediately upstream of each start site, which comprise the CREs A, B, and C, contain 42 fixed differences between ZAL2 and ZAL2^{m} (0.7% divergence; Fig. 4A and Table A6) (Sun, Huh, Zinzow-Kramer, Maney, & Yi, 2018). To test whether these genetic differences are sufficient to cause allelic differences in transcription activity, we performed luciferase reporter assays in avian cells in culture. All three CREs were cloned upstream of the luciferase gene in a vector containing an SV40 enhancer such that expression of the luciferase gene was under transcriptional control of the CREs (Fig. A3A). These constructs were transfected into DT40 cells, an avian cell line amenable to transfection (Buerstedde et al., 1990; Winding & Berchtold, 2001) (Table A7 and Fig. A3B). For all three CREs, the activity of the ZAL2^{m} allele was higher than that of the

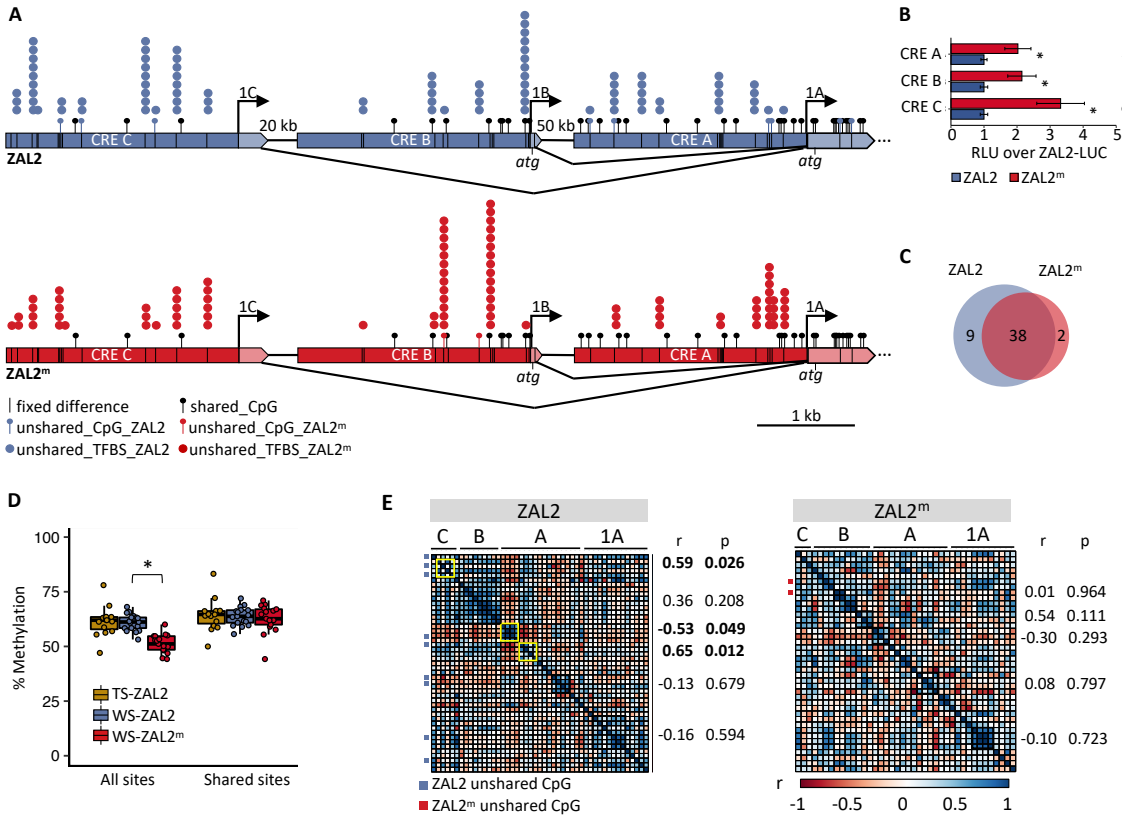

Figure 4. Mechanisms underlying allelic imbalance in *ESR1*. (A) *ESR1* is alternatively spliced. Dark blue or red regions are CREs; transcribed regions are light colors. Black lines within CREs represent 42 fixed differences distinguishing ZAL2 from ZAL2^{m}. Lollipops represent CpG sites. Stacked circles represent transcription factors that are expressed in TnA and for which a binding site is disrupted by a fixed difference. (B) *Cis*-regulatory variation in *ESR1* contributes to variation in activity of the CREs in avian DT40 cells *in vitro*. Activity, in RLU, of the ZAL2^{m}-LUC (red) and ZAL2-LUC (blue) constructs are shown normalized to activity of the ZAL2-LUC construct (± SEM). n = 6, * $P < 0.05$. See Table 8. (C) The Venn diagram shows the number of shared and unshared CpG sites within the CREs. (D) In TnA, methylation of these CREs depended on the allele. In WS birds, the ZAL2^{m} sequence was less methylated than ZAL2 but this difference was not detectable when considering only shared CpG sites (see Table 10). Boxplots indicate median, interquartile range, and 10th-90th percentiles (TS, n = 14, WS, n = 18). (E) Correlation matrices, using data from WS birds, demonstrates covariation in methylation of CpG sites along the sequences. Similarly methylated clusters that significantly predicted allele-specific expression are outlined in yellow; those that did not are outlined in black (see Fig. A4). Unshared sites are marked by boxes to the left of each matrix. * $P < 0.05$.

ZAL2 allele (Fig. 4B and A3; Table A7). This result suggests that the genetic differentiation between the alleles is sufficient to cause differential expression even in the absence of other factors (e.g., *trans*-regulatory elements or chromatin status) that may contribute to morph differences in expression.

To explore the impact of allelic differentiation on transcription factor binding, we identified transcription factor binding sites that are allele-specific, meaning that a SNP has either abolished the site or reduced its affinity for a particular transcription factor on one allele compared with the other. To identify such sites, we used sTRAP, a tool that predicts the impact of SNPs on the affinity of transcription factors (Manke et al., 2010). This approach yielded nearly 300 binding sites within the *ESR1* gene with differential affinity for the ZAL2 vs. ZAL2^{m} alleles ($P < 0.05$, Benjamini-Hochberg correction for multiple comparisons). Using our published RNA-seq data (Sun et al., 2018; Zinzow-Kramer et al., 2015), we found that 120 of those transcription factors are expressed in TnA in both morphs (Fig. 4A and A4), suggesting a clear mechanism by which the level of *ESR1* expression could be influenced by genotype. These transcription factors were neither overrepresented on ZAL2^{m} nor enriched for differential expression by morph (Fig. A4).

Differential gene expression and allelic imbalance do not always involve genetic differentiation. These phenomena can also be caused by epigenetic factors, such as DNA methylation. Of 49 CpG sites in the regulatory sequences of *ESR1* (Fig. 4A), 22% are 'unshared', meaning that they contain a SNP and thus are present on only one of the two alleles. The number of unshared CpGs is higher on ZAL2 (Fig. 4C; Table A8), suggesting that genetic divergence could contribute to differential methylation of the two alleles. To test this hypothesis, we sequenced bisulfite-converted DNA extracted from TnA of free-

living birds in breeding condition. This analysis revealed that the ZAL2 allele is in fact significantly more methylated than the ZAL2^{m} allele (Fig. 4D; Table A10), suggesting the morph difference in expression could be due in part to epigenetic control. The differential methylation could not be detected when we considered only shared sites, that is, CpG sites present on both alleles (Fig. 4D). Furthermore, methylation of the ZAL2 allele was essentially equivalent in the WS and TS birds (Fig. 4D). Therefore, differential methylation contributing to morph differences in expression likely occurs predominantly at genetically differentiated CpG sites, not at shared sites.

We next tested whether methylation of the CREs predicts expression for each allele. As a means of data reduction, we constructed correlation matrices of CpG methylation to identify clusters of similarly methylated neighboring sites within each allele (Figs. 4E and A5) following established protocols (Rubenstein et al., 2016; Siller & Rubenstein, 2019). These clusters varied according to allele (Fig. 4E), suggesting that genetic differentiation likely both contributed to and disrupted interactions between neighboring sites. Remarkably, of the three clusters that significantly predicted allele-specific expression, all contained at least one unshared CpG site and all were on ZAL2 rather than ZAL2^{m}. Thus, the predictive value of methylated CpG sites was markedly reduced for ZAL2^{m}, which is missing the ZAL2-specific sites. Our findings show that this system represents a rare and interesting example of *cis*-regulation that is attributable to a combination of genetic and epigenetic forces (Okhovat, Berrio, Wallace, Ophir, & Phelps, 2015). The regulatory variation in *ESR1* predicts and likely causes differential expression of this gene, which as we showed above, can drive divergent behavioral phenotypes.

Discussion

In this series of studies, we have demonstrated how genetic divergence in a single gene has contributed to the evolution of an aggressive phenotype in a naturally-occurring wild species of vertebrate. The gene *ESR1* has been captured by a chromosomal rearrangement that comprises a supergene, a group of linked genes that are co-inherited. Supergenes caused by inversions are associated with social behavior not only in white-throated sparrows but also in ruffs, Alpine silver ants, and fire ants (Kupper et al., 2016; Purcell, Brelsford, Wurm, Perrin, & Chapuisat, 2014; Wang et al., 2013). The genes captured inside these inversions are in tight linkage disequilibrium, making it difficult to identify causal alleles or to uncover the genetic and epigenetic mechanisms that affect their expression (Rubenstein et al., 2019; Wellenreuther & Bernatchez, 2018). Here we show that identifying such alleles is possible when genomic resources are available, the model is amenable to mechanistic experimental approaches, and there is already some knowledge of the physiological mechanisms underlying the behavior—in this case, steroid hormones.

We previously showed that in white-throated sparrows, *ESR1* is expressed not only in TnA but also in other regions of the brain thought to regulate social behavior (Horton, Hudson, et al., 2014). Although *ESR1* expression depends on morph in most of these regions, the direction of that effect varies. In other words, in some regions expression is higher in WS birds, whereas in other regions it is higher in TS birds. For example, in contrast to its expression in TnA, *ESR1* expression in the rPOM is higher in TS males than in WS males in both nestlings and adults (Grogan et al., 2019; Horton, Hudson, et al., 2014). In parental adult males, this expression in the rPOM predicts

parental provisioning more accurately than does morph, suggesting a potentially causal role for *ESR1* expression in parenting (Horton, Hudson, et al., 2014). This relationship between *ESR1* and parental behavior was detected only in the rPOM, not in any other region in which *ESR1* expression was measured. Clearly, the potential influence of *ESR1* on any particular behavior depends not only on the level at which the gene is expressed, but also on where it is expressed; in other words, expression must be influenced by local, region-specific conditions. In the present study, we have shown that these local factors dictate allelic expression. In both adults and nestlings, the ZAL2^{m} allele of *ESR1* is expressed at higher levels in TnA whereas expression of the ZAL2 allele is greater in the HYP and rPOM (Fig. 3). These findings suggest that *cis*-regulatory variation interacts with region-dependent *trans*-regulatory and epigenetic factors to create complex patterns of expression that lead to rich phenotypic variation. Because of its well-characterized ZAL2/ZAL2^{m} system, the white-throated sparrow is an excellent model for exploring this interesting interplay between genetic and epigenetic regulation of social behavior.

The adaptive value of chromosomal inversions has been the subject of much interest and debate for nearly a century (Theodosius Dobzhansky, 1970; Kirkpatrick, 2010; Sturtevant, 1921; Wellenreuther & Bernatchez, 2018). Because they suppress recombination, inversions can link co-adapted alleles together, ensuring co-inheritance (Theodosius Dobzhansky, 1970; Th Dobzhansky & Sturtevant, 1938). In other words, an inversion can lock together alleles that interact well with each other, benefiting the individual and the alleles alike. Because it is a transcription factor, ERα interacts with a large number of other proteins as well as with regulatory elements of many other genes. Thus, the ZAL2^{m} allele of *ESR1* is likely to be co-evolving with other genes inside the

supergene. One potential co-evolving gene is *GRM1*, encoding the metabotropic glutamate receptor mGluR, which in rats interacts with ERα situated in cell membranes (Dewing et al., 2007). This possibility is particularly intriguing because the time course of the behavioral effects of E2 administration we observed in this study strongly suggest a nongenomic, rather than genomic, mechanism of action (see also (Heimovics et al., 2018; Merritt et al., 2018)). Also inside the supergene are the genes *NCOA7*, encoding nuclear receptor coactivator 7, and *TBP,* encoding the TATA box-binding protein, both of which interact directly with ERα as transcriptional co-activators (Lazennec, Ediger, Petz, Nardulli, & Katzenellenbogen, 1997). Our gene network analysis of expression in TnA showed that *ESR1* is itself a well-connected 'hub' within a module of 157 genes that are differentially expressed between the morphs and that predict territorial singing (Zinzow-Kramer et al., 2015). Of these 157 genes, 115 are inside the ZAL2^{m} supergene. Thus we believe that there is great potential in this system to identify co-adapted genes and to show how they have co-evolved inside the supergene.

Linking co-adapted alleles is just one of several hypothesized functions of inversions. For example, inversions may capture locally adapted alleles (Kirkpatrick & Barton, 2006) or contribute to speciation (Navarro & Barton, 2003). The ZAL2/2^{m} arrangement in white-throated sparrows is a special case, however, because of the strong disassortative mating. Nearly every breeding pair consists of one WS and one TS bird (Horton et al., 2013; Tuttle et al., 2016), meaning that the supergene is maintained by social behavior itself (Rubenstein et al., 2019) independent of geography or local conditions. Clearly, ZAL2^{m} is not driving a speciation event nor has it spread because it is favored in particular environments. Instead, these heteromorphic chromosomes seem to

be more akin to early-evolving sex chromosomes (Falls & Kopachena, 2020; Sun et al., 2018). Inversions are common on sex chromosomes, perhaps because they capture sex-determining genes together with alleles that benefit a particular sex; in other words they can bind together a male-determining gene with alleles that enhance male fitness (Charlesworth, 1991). Thus, inversions are particularly adaptive in the case of antagonistic selection, in which certain alleles are beneficial to only one of two alternative life-history strategies, e.g., male or female. We hypothesize that in white-throated sparrows, the ZAL2^{m} arrangement harbors a collection of alleles beneficial to the WS strategy, characterized by increased territorial aggression and low parenting, whereas the ZAL2 harbors alleles that favor the TS strategy.

We recently reported that expression of the gene for vasoactive intestinal peptide (*VIP*), located only 345 kb away from *ESR1*, differs between the morphs and predicts behavior (Horton, Michael, Prichard, & Maney, 2020). WS birds of both sexes have higher levels of *VIP* expression in the anterior hypothalamus, a region in which *VIP* expression is causal for aggression in violet-eared waxbills (Goodson, Kelly, Kingsbury, & Thompson, 2012). In parental white-throated sparrows, TS birds have higher levels of *VIP* expression in the infundibular region (Horton et al., 2020), which contains the *VIP* cell population that controls prolactin release (Maney, Schoech, Sharp, & Wingfield, 1999). We fully expect that additional genes will be shown to contribute to the alternative life-history strategies of the WS and TS morphs and that this species represents an important model with which to understand the role of *cis*-regulatory variation in the evolution of behavior.

References

Anders, S., Pyl, P. T., & Huber, W. (2015). HTSeq—a Python framework to work with high-throughput sequencing data. *Bioinformatics, 31*(2), 166-169.

Bates, D., Mächler, M., Bolker, B., & Walker, S. (2014). Fitting linear mixed-effects models using lme4. *arXiv preprint arXiv:1406.5823*.

Bendesky, A., & Bargmann, C. I. (2011). Genetic contributions to behavioural diversity at the gene-environment interface. *Nature Reviews: Genetics, 12*(12), 809-820.

Bendesky, A., Kwon, Y. M., Lassance, J. M., Lewarch, C. L., Yao, S., Peterson, B. K., . . . Hoekstra, H. E. (2017). The genetic basis of parental care evolution in monogamous mice. *Nature, 544*(7651), 434-439.

Buerstedde, J., Reynaud, C., Humphries, E., Olson, W., Ewert, D., & Weill, J. (1990). Light chain gene conversion continues at high rate in an ALV-induced cell line. *EMBO Journal, 9*(3), 921-927.

Charlesworth, B. (1991). The evolution of sex chromosomes. *Science, 251*(4997), 1030-1033.

Chen, X., Weaver, J., Bove, B. A., Vanderveer, L. A., Weil, S. C., Miron, A., . . . Godwin, A. K. (2008). Allelic imbalance in *BRCA1* and *BRCA2* gene expression is associated with an increased breast cancer risk. *Human Molecular Genetics, 17*(9), 1336-1348.

Cheng, M.-F., Chaiken, M., Zuo, M., & Miller, H. (1999). Nucleus taenia of the amygdala of birds: anatomical and functional studies in ring doves (*Streptopelia risoria*) and European starlings (*Sturnus vulgaris*). *Brain, Behavior and Evolution, 53*(5-6), 243-270.

Davis, J. K., Mittel, L. B., Lowman, J. J., Thomas, P. J., Maney, D. L., Martin, C. L., . . . Thomas, J. W. (2011). Haplotype-based genomic sequencing of a chromosomal polymorphism in the white-throated sparrow (*Zonotrichia albicollis*). *Journal of Heredity, 102*(4), 380-390.

Dewing, P., Boulware, M. I., Sinchak, K., Christensen, A., Mermelstein, P. G., & Micevych, P. (2007). Membrane estrogen receptor-α interactions with metabotropic glutamate receptor 1a modulate female sexual receptivity in rats. *Journal of Neuroscience, 27*(35), 9294-9300.

Dobin, A., Davis, C. A., Schlesinger, F., Drenkow, J., Zaleski, C., Jha, S., . . . Gingeras, T. R. (2013). STAR: ultrafast universal RNA-seq aligner. *Bioinformatics, 29*(1), 15-21.

Dobzhansky, T. (1970). *Genetics of the Evolutionary Process* (Vol. 139): Columbia University Press.

Dobzhansky, T., & Sturtevant, A. H. (1938). Inversions in the chromosomes of *Drosophila pseudoobscura*. *Genetics, 23*(1), 28.

Falls, J. B., & Kopachena, J. G. (2020). White-throated sparrow (*Zonotrichia albicollis*), version 3.0. In A. F. Poole (Ed.), *The Birds of North America*.

Fox, J., & Weisberg, S. (2011). Multivariate linear models in R. *An R Companion to Applied Regression. Los Angeles: Thousand Oaks*.

Geiger, T., Wehner, A., Schaab, C., Cox, J., & Mann, M. (2012). Comparative proteomic analysis of eleven common cell lines reveals ubiquitous but varying expression of most proteins. *Molecular and Cellular Proteomics, 11*(3), M111.014050.

Goodson, J. L., Kelly, A. M., Kingsbury, M. A., & Thompson, R. R. (2012). An aggression-specific cell type in the anterior hypothalamus of finches. *Proceedings of the National Academy of Sciences of the United States of America, 109*(34), 13847-13852.

Griffiths, R., Double, M. C., Orr, K., & Dawson, R. J. (1998). A DNA test to sex most birds. *Molecular Ecology, 7*(8), 1071-1075.

Grogan, K. E., Horton, B. M., Hu, Y., & Maney, D. L. (2019). A chromosomal inversion predicts the expression of sex steroid-related genes in a species with alternative behavioral phenotypes. *Molecular and Cellular Endocrinology, 495*, 110517.

Heimovics, S. A., Ferris, J. K., & Soma, K. K. (2015). Non-invasive administration of 17β-estradiol rapidly increases aggressive behavior in non-breeding, but not breeding, male song sparrows. *Hormones and Behavior, 69*, 31-38.

Heimovics, S. A., Merritt, J. R., Jalabert, C., Ma, C., Maney, D. L., & Soma, K. K. (2018). Rapid effects of 17beta-estradiol on aggressive behavior in songbirds: environmental and genetic influences. *Hormones and Behavior, 104*, 41-51.

Horton, B. M., Hauber, M. E., & Maney, D. L. (2012). Morph matters: aggression bias in a polymorphic sparrow. *PLoS ONE, 7*(10), e48705.

Horton, B. M., Hu, Y., Martin, C. L., Bunke, B. P., Matthews, B. S., Moore, I. T., . . . Maney, D. L. (2013). Behavioral characterization of a white-throated sparrow homozygous for the ZAL2m chromosomal rearrangement. *Behavior Genetics, 43*(1), 60-70.

Horton, B. M., Hudson, W. H., Ortlund, E. A., Shirk, S., Thomas, J. W., Young, E. R., . . . Maney, D. L. (2014). Estrogen receptor alpha polymorphism in a species with

alternative behavioral phenotypes. *Proceedings of the National Academy of Sciences of the United States of America, 111*(4), 1443-1448.

Horton, B. M., Michael, C. M., Prichard, M. R., & Maney, D. L. (2020). Vasoactive intestinal peptide as a mediator of the effects of a supergene on social behaviour. *Proceedings of the Royal Society B, 287*(1924), 20200196.

Horton, B. M., Moore, I. T., & Maney, D. L. (2014). New insights into the hormonal and behavioural correlates of polymorphism in white-throated sparrows, *Zonotrichia albicollis*. *Animal Behaviour, 93*, 207-219.

Huynh, L. Y., Maney, D. L., & Thomas, J. W. (2011). Chromosome-wide linkage disequilibrium caused by an inversion polymorphism in the white-throated sparrow (*Zonotrichia albicollis*). *Heredity (Edinb), 106*(4), 537-546.

Kelly, A. M., & Goodson, J. L. (2014). Hypothalamic oxytocin and vasopressin neurons exert sex-specific effects on pair bonding, gregariousness, and aggression in finches. *Proceedings of the National Academy of Sciences of the United States of America, 111*(16), 6069-6074.

Ketterson, E. D., & Nolan, V. (1992). Hormones and life histories: an integrative approach. *The American Naturalist, 140*, S33-S62.

Kim, S. (2015). ppcor: an R package for a fast calculation to semi-partial correlation coefficients. *Communications for Statistical Applications and Methods, 22*(6), 665.

Kim, S., & Yi, S. V. (2007). Understanding relationship between sequence and functional evolution in yeast proteins. *Genetica, 131*(2), 151-156.

Kirkpatrick, M. (2010). How and why chromosome inversions evolve. *PLoS Biology, 8*(9).

Kirkpatrick, M., & Barton, N. (2006). Chromosome inversions, local adaptation and speciation. *Genetics, 173*(1), 419-434.

Krueger, F. (2015). Trim galore: A wrapper tool around Cutadapt and FastQC to consistently apply quality and adapter trimming to FastQ files. *516*, 517.

Krueger, F., & Andrews, S. R. (2011). Bismark: a flexible aligner and methylation caller for Bisulfite-Seq applications. *Bioinformatics, 27*(11), 1571-1572.

Krueger, F., & Andrews, S. R. (2016). SNPsplit: Allele-specific splitting of alignments between genomes with known SNP genotypes. *F1000 Res., 5*, 1479.

Kupper, C., Stocks, M., Risse, J. E., Dos Remedios, N., Farrell, L. L., McRae, S. B., . . . Burke, T. (2016). A supergene determines highly divergent male reproductive morphs in the ruff. *Nature Genetics, 48*(1), 79-83.

Ladjali-Mohammedi, K., Bitgood, J., Tixier-Boichard, M., & De Leon, F. P. (1999). International system for standardized avian karyotypes (ISSAK): standardized banded karyotypes of the domestic fowl (*Gallus domesticus*). *Cytogenetic and Genome Research, 86*(3-4), 271-276.

Lamichhaney, S., Fan, G., Widemo, F., Gunnarsson, U., Thalmann, D. S., Hoeppner, M. P., . . . Andersson, L. (2016). Structural genomic changes underlie alternative reproductive strategies in the ruff (*Philomachus pugnax*). *Nature Genetics, 48*(1), 84-88.

Langmead, B., & Salzberg, S. L. (2012). Fast gapped-read alignment with Bowtie 2. *Nature Methods, 9*(4), 357.

Lazennec, G., Ediger, T. R., Petz, L. N., Nardulli, A. M., & Katzenellenbogen, B. S. (1997). Mechanistic aspects of estrogen receptor activation probed with constitutively active estrogen receptors: correlations with DNA and coregulator interactions and receptor conformational changes. *Molecular Endocrinology, 11*(9), 1375-1386.

Love, M. I., Huber, W., & Anders, S. (2014). Moderated estimation of fold change and dispersion for RNA-seq data with DESeq2. *Genome biology, 15*(12), 550.

Madrid, J. E., Parker, K. J., & Ophir, A. G. (2020). Variation, plasticity, and alternative mating tactics: revisiting what we know about the socially monogamous prairie vole. *Advances in the Study of Behavior*, 203.

Maney, D. L. (2008). Endocrine and genomic architecture of life history trade-offs in an avian model of social behavior. *General and Comparative Endocrinology, 157*(3), 275-282.

Maney, D. L., Horton, B. M., & Zinzow-Kramer, W. M. (2015). Estrogen receptor alpha as a mediator of life-history trade-offs. *Integrative and Comparative Biology, 55*(2), 323-331.

Maney, D. L., Lange, H. S., Raees, M. Q., Reid, A. E., & Sanford, S. E. (2009). Behavioral phenotypes persist after gonadal steroid manipulation in white-throated sparrows. *Hormones and Behavior, 55*(1), 113-120.

Maney, D. L., Schoech, S. J., Sharp, P. J., & Wingfield, J. C. (1999). Effects of vasoactive intestinal peptide on plasma prolactin in passerines. *General and Comparative Endocrinology, 113*(3), 323-330.

Manke, T., Heinig, M., & Vingron, M. (2010). Quantifying the effect of sequence variation on regulatory interactions. *Human Mutation, 31*(4), 477-483.

Matragrano, L. L., LeBlanc, M. M., Chitrapu, A., Blanton, Z. E., & Maney, D. L. (2013). Testosterone alters genomic responses to song and monoaminergic innervation of auditory areas in a seasonally breeding songbird. *Developmental neurobiology, 73*(6), 455-468.

Mello, C. V., Kaser, T., Buckner, A. A., Wirthlin, M., & Lovell, P. V. (2019). Molecular architecture of the zebra finch arcopallium. *Journal of Comparative Neurology*.

Merritt, J. R. (2019). Evolution of behavior: Genotype to phenotype. In J. C. Choe (Ed.), *Encyclopedia of Animal Behavior* (2nd ed., Vol. 2, pp. 234-242): Elsevier, Academic Press.

Merritt, J. R., Davis, M. T., Jalabert, C., Libecap, T. J., Williams, D. R., Soma, K. K., & Maney, D. L. (2018). Rapid effects of estradiol on aggression depend on genotype in a species with an estrogen receptor polymorphism. *Hormones and Behavior, 98*, 210-218.

Merritt, J. R., Grogan, K. E., Zinzow-Kramer, W. M., Sun, D., Ortlund, E. A., Yi, S. V., & Maney, D. L. (2020). A supergene-linked estrogen receptor drives alternative phenotypes in a polymorphic songbird. *Proceedings of the National Academy of Sciences of the United States of America*. Advance online publication. DOI: www.pnas.org/cgi/doi/10.1073/pnas.2011347117.

Navarro, A., & Barton, N. H. (2003). Accumulating postzygotic isolation genes in parapatry: a new twist on chromosomal speciation. *Evolution, 57*(3), 447-459.

Niepoth, N., & Bendesky, A. (2020). How natural genetic variation shapes behavior. *Annual Review of Genomics and Human Genetics, 21*.

Ogawa, S., Lubahn, D. B., Korach, K. S., & Pfaff, D. W. (1997). Behavioral effects of estrogen receptor gene disruption in male mice. *Proceedings of the National Academy of Sciences of the United States of America, 94*(4), 1476-1481.

Okhovat, M., Berrio, A., Wallace, G., Ophir, A. G., & Phelps, S. M. (2015). Sexual fidelity trade-offs promote regulatory variation in the prairie vole brain. *Science, 350*(6266), 1371-1374.

Okhovat, M., Maguire, S. M., & Phelps, S. M. (2017). Methylation of *AVPR1A* in the cortex of wild prairie voles: effects of CpG position and polymorphism. *Royal Society Open Science, 4*(1), 160646.

Palkovits, M. (1973). Isolated removal of hypothalamic or other brain nuclei of the rat. *Brain Research, 59*, 449-450.

Purcell, J., Brelsford, A., Wurm, Y., Perrin, N., & Chapuisat, M. (2014). Convergent genetic architecture underlies social organization in ants. *Current Biology, 24*(22), 2728-2732.

Reiner, A., Perkel, D. J., Bruce, L. L., Butler, A. B., Csillag, A., Kuenzel, W., . . . Striedter, G. (2004). Revised nomenclature for avian telencephalon and some related brainstem nuclei. *Journal of Comparative Neurology, 473*(3), 377-414.

Robinson, G. E., Grozinger, C. M., & Whitfield, C. W. (2005). Sociogenomics: Social life in molecular terms. *Nature Reviews: Genetics, 6*(4), 257-270.

Romanov, M. N., Dodgson, J. B., Gonser, R. A., & Tuttle, E. M. (2011). Comparative BAC-based mapping in the white-throated sparrow, a novel behavioral genomics model, using interspecies overgo hybridization. *BMC research notes, 4*(1), 211.

Rosvall, K. A., Bergeon Burns, C. M., Barske, J., Goodson, J. L., Schlinger, B. A., Sengelaub, D. R., & Ketterson, E. D. (2012). Neural sensitivity to sex steroids predicts individual differences in aggression: implications for behavioural evolution. *Proceedings of the Royal Society B, 279*(1742), 3547-3555.

Rubenstein, D. R., Agren, J. A., Carbone, L., Elde, N. C., Hoekstra, H. E., Kapheim, K. M., . . . Hofmann, H. A. (2019). Coevolution of genome architecture and social behavior. *Trends in Ecology & Evolution*.

Rubenstein, D. R., Skolnik, H., Berrio, A., Champagne, F. A., Phelps, S., & Solomon, J. (2016). Sex-specific fitness effects of unpredictable early life conditions are associated with DNA methylation in the avian glucocorticoid receptor. *Molecular Ecology, 25*(8), 1714-1728.

Russell, L. (2018). Emmeans: estimated marginal means, aka least-squares means. *R package version, 1*(2).

Siller, S. J., & Rubenstein, D. R. (2019). A tissue comparison of DNA methylation of the glucocorticoid receptor gene (*NR3C1*) in European starlings. *Integrative and Comparative Biology, 59*(2), 264-272.

Snyder-Mackler, N., & Tung, J. (2017). Vasopressin and the neurogenetics of parental care. *Neuron, 95*(1), 9-11.

Stetzik, L., Ganshevsky, D., Lende, M. N., Roache, L. E., Musatov, S., & Cushing, B. S. (2018). Inhibiting ERα expression in the medial amygdala increases prosocial

behavior in male meadow voles (*Microtus pennsylvanicus*). *Behavioural Brain Research, 351*, 42-48.

Sturtevant, A. (1921). A case of rearrangement of genes in Drosophila. *Proceedings of the National Academy of Sciences of the United States of America, 7*(8), 235.

Sun, D., Huh, I., Zinzow-Kramer, W. M., Maney, D. L., & Yi, S. V. (2018). Rapid regulatory evolution of a nonrecombining autosome linked to divergent behavioral phenotypes. *Proceedings of the National Academy of Sciences of the United States of America, 115*(11), 2794-2799.

Sun, D., Layman, T., Jeong, H., Chatterjee, P., Grogan, K. E., Merritt, J. R., . . . Yi, S. V. (2020). Genome-wide variation in DNA methylation linked to developmental stage and chromosomal suppression of recombination in white-throated sparrows. *bioRxiv*.

Symonds, M. R., & Moussalli, A. (2011). A brief guide to model selection, multimodel inference and model averaging in behavioural ecology using Akaike's information criterion. *Behavioral Ecology and Sociobiology, 65*(1), 13-21.

Thomas, J. W., Caceres, M., Lowman, J. J., Morehouse, C. B., Short, M. E., Baldwin, E. L., . . . Martin, C. L. (2008). The chromosomal polymorphism linked to variation in social behavior in the white-throated sparrow (*Zonotrichia albicollis*) is a complex rearrangement and suppressor of recombination. *Genetics, 179*(3), 1455-1468.

Thorneycroft, H. (1966). Chromosomal polymorphism in the white-throated sparrow, *Zonotrichia albicollis* (Gmelin). *Science, 154*(3756), 1571-1572.

Thorneycroft, H. (1975). A cytogenetic study of the white-throated sparrow, *Zonotrichia albicollis* (Gmelin). *Evolution*, 611-621.

Trainor, B. C., Kyomen, H. H., & Marler, C. A. (2006). Estrogenic encounters: how interactions between aromatase and the environment modulate aggression. *Frontiers in Neuroendocrinology, 27*(2), 170-179.

Tuttle, E. M., Bergland, A. O., Korody, M. L., Brewer, M. S., Newhouse, D. J., Minx, P., . . . Balakrishnan, C. N. (2016). Divergence and functional degradation of a sex chromosome-like supergene. *Current Biology, 26*(3), 344-350.

Wang, J., Wurm, Y., Nipitwattanaphon, M., Riba-Grognuz, O., Huang, Y.-C., Shoemaker, D., & Keller, L. (2013). A Y-like social chromosome causes alternative colony organization in fire ants. *Nature, 493*(7434), 664.

Wellenreuther, M., & Bernatchez, L. (2018). Eco-evolutionary genomics of chromosomal inversions. *Trends in Ecology & Evolution, 33*(6), 427-440.

Wilson, E. O. (2000). *Sociobiology: The new synthesis*: Harvard University Press.

Winding, P., & Berchtold, M. W. (2001). The chicken B cell line DT40: a novel tool for gene disruption experiments. *Journal of Immunological Methods, 249*(1-2), 1-16.

Wingfield, J. C., Hegner, R. E., Dufty, A. M., & Ball, G. F. (1990). The "challenge hypothesis": theoretical implications for patterns of testosterone secretion, mating systems, and breeding strategies. *American Naturalist, 136*(6), 829-846.

Zeileis, A., & Hothorn, T. (2002). Diagnostic checking in regression relationships.

Zinzow-Kramer, W. M., Horton, B. M., & Maney, D. L. (2014). Evaluation of reference genes for quantitative real-time PCR in the brain, pituitary, and gonads of songbirds. *Hormones and Behavior, 66*(2), 267-275.

Zinzow-Kramer, W. M., Horton, B. M., McKee, C. D., Michaud, J. M., Tharp, G. K., Thomas, J. W., . . . Maney, D. L. (2015). Genes located in a chromosomal inversion are correlated with territorial song in white-throated sparrows. *Genes, Brain and Behavior, 14*(8), 641-654.

Appendix

Data Availability and Acknowledgments

Sequencing data reported in this manuscript are deposited in the National Center for Biotechnology Information under accession PRJNA647725. This work is in press at the Proceedings of the National Academy of the United States of America (Merritt et al., 2020). We thank Carlos Rodriguez-Saltos, T.J. Libecap, Suzanne Mays, William Hudson, Emily Kim, and Aubrey Kelly for technical assistance. This work was supported by NIH Grant 1R01MH082833 to D.L.M, NSF Grant 16-505 to D.L.M, and NIH Grant 1F31MH114509 to J.R.M.

Effects of *ESR1* knockdown on aggression

Non-breeding white-throated sparrows. We collected 33 white-throated sparrows in mist nets on the campus of Emory University in Atlanta, GA during fall migration, when gonads are regressed and plasma levels of steroid hormones are low (Maney, 2008; Matragrano et al., 2013). Our rationale for testing birds in non-breeding condition was first that the morph difference in *ESR1* expression in nucleus taenia of the amygdala (TnA) is pronounced in non-breeding birds (Grogan et al., 2019; Maney et al., 2015), and second that ERα would be relatively unoccupied and sensitive to exogenous estradiol (E2) (Merritt et al., 2018). Sex and morph were confirmed by PCR (Griffiths, Double, Orr, & Dawson, 1998; Thomas et al., 2008). Birds were housed in the Emory animal care facility in walk-in flight cages (4’ x 7’ x 6’), supplied with *ad libitum* seed and water. The day length was kept constant at 10L:14D to prevent spontaneous gonadal recrudescence. At least one month prior to behavioral assays, birds were transferred to

individual cages (15” x 15” x 17”) inside identical walk-in sound-attenuating booths (Industrial Acoustics, Bronx, NY), two to six birds per booth. In order to habituate birds to the presentation of wax moth larvae (*Achroia grisella*) as food items, which would be used in the E2 manipulation, each bird received one larva per day. Birds that consistently and reliably ate the larva within one min of presentation were included in the study.

Cannulation surgeries. Each bird was fitted with bilateral 26 gauge, stainless steel guide cannulae aimed at TnA. Surgeries were performed using a stereotaxic apparatus with ear bars and beak holder custom-designed for birds. To place the cannulae we used a custom-designed holder that accommodates two cannulae with a fixed distance of 3.8 mm between them (PlasticsOne, Roanoke, VA). Four animals were used to establish stereotaxic coordinates and proper angles of approach for TnA. Final coordinates, relative to the anterior pole of the cerebellum, were AP 0.0 mm, ML 1.9 mm. Cannulae were lowered to a depth of 3.6mm and mounted to the skull using dental acrylic and veterinary-grade tissue adhesive (VetBond; 3M). A 33-gauge stainless steel obturator, which extended 1 mm beyond the tip of the guide cannula, was inserted on each side. Birds recovered from surgery for at least 3 days before dominance testing (see next section).

Pre-screening for social dominance. To quantify aggression, we presented each focal animal with a subordinate “opponent” in an adjacent cage. In order to ensure that each opponent was subordinate to the focal animal, we pre-screened the birds in dyads to determine their dominance relationships. This screening was performed according to Merritt et al. (2018). Briefly, during pre-screening trials, we placed the cages of two same-morph, cannulated birds adjacent to one another in an otherwise empty sound-

attenuating booth equipped with a video camera ~1m from their cages. We recorded their interactions for 30 min, then returned each bird to its home booth. Each dyad was tested once. Dominance was operationalized according to Merritt et al. (2018). An observer scored the videos for two behaviors: attempted attacks by both birds, defined as the bird making contact with both feet on the wall of its cage facing the other bird and flapping its wings, and the amount of time (s) each bird spent in proximity to the other cage. Proximity was defined as being within an area ~12cm from the wall of the cage closest to the other bird (Fig. 2B). This area was marked on each focal animal's cage and visible in the videos. The member of the dyad that attacked more and spent more time in proximity to the other bird's cage was deemed dominant (Merritt et al., 2018). In this study, the dominant bird made at least 30% more attacks (average 82.2% more) and spent at least 5% more time in proximity to the other bird's cage (average 33.9% more). In the behavioral trials described below, the dominant bird was used as the focal animal and the subordinate was the opponent. If neither bird in the dyad dominated in terms of both behaviors, the dyad was dissolved and each bird was tested again with a new bird. Most dyads were same-sex; however, some dyads consisted of a male focal animal and a female opponent. No female engaged in copulation solicitation or other courtship behavior during testing, and whether the dyad was same-sex or mixed-sex did not affect the behavior of either the focal animal (attacks $F(1,25) = 0.00$, $P = 0.985$; time $F(1,25) = 0.51$, $P = 0.484$) or the opponent (attacks $F(1,25) = 0.08$, $P = 0.78$; time $F(1,25) = 1.68$, $P = 0.21$). We emphasize that all birds were in non-breeding condition and did not engage in courtship behavior during study.

Antisense. *ESR1* expression was manipulated with custom-designed LNA 15-mer antisense oligonucleotides designed by Qiagen following Kelly & Goodson (Kelly & Goodson, 2014). The antisense oligo for *ESR1*-KD (TTCAAAGGTGGCACT) was designed to target the stop codon of the *ESR1* transcript (XM_026794125.1), avoiding ZAL2/ZAL2^{m} SNPs, starting 11 bp upstream of the stop codon. A scrambled control oligonucleotide was designed from the same nucleotides, but in a random order (TAGCATGTCAGATCG). Both the *ESR1*-KD and scrambled sequences were searched on BLAST (NCBI) against the *Zonotrichia albicollis* refseq_rna to confirm no significant alignments to other transcripts, in particular *ESR2* (XM_014270428.2).

Starting the day after the establishment of a dyad, we made a series of four infusions of antisense or scrambled oligos (1 µg in 0.25 µl isotonic saline), 2 per day, 10 hrs apart (within the first and last hour of light of the light/dark cycle). 250 nl of solution was infused slowly (2 min per side to avoid tissue damage) using a Hamilton neurosyringe connected to a 33 gauge injector via ~20 cm of polyethylene tubing. Cannulae were checked after each infusion and no leakage was noted.

Hormone manipulation. We administered exogenous E2 via a non-invasive, minimally stressful method that increases plasma E2 to a similar, high level in both morphs (Merritt et al., 2018). Before behavioral testing (below), a wax moth larva was injected with either 300 µg of cyclodextrin-encapsulated E2 (Sigma-Aldrich, cat. no. E4389) or cyclodextrin alone (CON; Sigma-Aldrich, cat no. C0926) using a Hamilton syringe. The injected larva was then fed to the focal animal. This oral dosage of E2 increases plasma E2 to a similar extent in WS and TS birds, and produces levels typical of breeding WS females (Merritt et al., 2018).

Behavioral testing. Behavioral testing was conducted the day after the fourth infusion, as previously described (Merritt et al., 2018). Briefly, before a behavioral trial, we placed the focal bird in its cage in an empty sound-attenuating booth to acclimate it to that environment. After one hr, we placed the opponent, in its cage, immediately adjacent to the focal bird's cage. An opaque barrier visually isolated the birds from each other. At the same time, a wax moth larva that had been injected immediately prior with E2 or CON was placed on the floor of the focal bird's cage and the experimenter immediately left the room. The birds were then monitored remotely to determine exactly when they consumed the larvae.

Ten min after the focal bird consumed the larva, the opaque barrier was removed and the birds were allowed to interact for 10 min. Attacks and time spent in proximity to the opponent were scored in de-identified videos, as described above for the pre-screening dominance trials, by an observer blind to morph (which is not easily assessed in videos), oligo type (antisense or scrambled), and hormone treatment (E2 or CON). As has been reported elsewhere (Heimovics, Ferris, & Soma, 2015; Merritt et al., 2018), singing occurred too infrequently for statistical analysis. After a washout period of 48 hrs, each focal bird participated in a second trial with the opposite hormone treatment (CON or E2). All trials were counterbalanced with respect to the order of treatment.

Data were analyzed as described by Merritt et al. (2018) using GLMs with a Gaussian distribution. When models specified an interaction term (morph × treatment or antisense × treatment), log-likelihood ratio tests were conducted on GLMs that included or excluded the interaction term with the function *lrtest* from the *lmtest* (v. 0.9.37) package (Table A2) (Zeileis & Hothorn, 2002). AIC values are reported in Table A2

(Symonds & Moussalli, 2011). Wald chi-squared tests were used to generate analysis-of-deviance summary tables. These analyses were performed with the function *glm* from the *lme4* (v. 1.1-15) package (Bates, Mächler, Bolker, & Walker, 2014) and summarized using the function *Anova* from the *car* (v.3.0-3) package (Fox & Weisberg, 2011). All analyses included the fixed effect of minute (1-10, over the course of the 10 min trial) and the random effect of individual.

Verification of cannula placement. Birds were euthanized by isoflurane overdose (Abbott Laboratories, North Chicago, IL) 24 hrs after the second behavioral trial. Each cannula was then injected with bromophenol blue. Brains were dissected from the skulls, frozen rapidly on dry ice, and sectioned on a cryostat at 300 μm in order to verify cannula placement and dissect tissue for qPCR. We then used the Palkovits punch technique (Palkovits, 1973) to obtain 1 mm diameter samples, as described by Grogan et al. (2019) and Zinzow-Kramer et al. (2015), at the site of the dye. We collected one punch per hemisphere for a total of 2 punches per bird. We considered birds with no dye in TnA to be misses (n = 7), and in these cases an additional 2 punches were made in TnA. Misses were determined by an observer blind to morph and oligo type (antisense or scrambled). The final sample size for each group, each of which included multiple males and females, was WS *ESR1*-KD n = 6, WS scrambled n = 7, TS *ESR1*-KD n = 6, TS scrambled n = 7.

RNA was extracted from the punches of TnA using the Qiagen miRNeasy micro kit (Qiagen, Valencia, CA, USA) with modifications described by Zinzow-Kramer et al. (2015). cDNA was produced by reverse transcription using the Transcriptor First Strand cDNA synthesis kit with random hexamer primers, then the reaction was diluted to 20

ng/µl for qPCR. We designed exon-spanning primers to be used with probes from the Roche Universal Probe Library for *ESR1* (Grogan et al., 2019) (F: GCACCTAACCTGTTACTGGACA; R: TGAAGGTTCATCATGCGAAA; Probe 132) and *ESR2* (F: GAAGCTGCAGCACAAGGAGT; R: CCTCTGCTGACCAGTGGAAC; Probe 151). The amplified sequence for *ESR2* was verified via agarose gel and Sanger sequencing. qPCR was performed using a Roche LightCycler 480 Real-Time PCR System in triplicate for each sample on 384-well plates as previously described (Zinzow-Kramer et al., 2015). Using the LightCycler 480 Software Version 1.5.0, we calculated crossing point (Cp) values using the Abs Quant/2nd Derivative Max method. We normalized the expression of each gene of interest to two reference genes: *PPIA* and *GAPDH*, which have been previously validated for use in white-throated sparrow brain tissue (Zinzow-Kramer, Horton, & Maney, 2014). We performed GLMs, as chosen on the basis of AIC values (Symonds & Moussalli, 2011), to test for effects of morph and oligo type (antisense or scrambled) on the expression of *ESR1*, and then followed up the significant interaction with GLMs testing for an effect of oligo type on expression of *ESR1* within each morph. Wald chi-squared tests were used to generate analysis-of-deviance summary tables. We used Pearson's partial correlations to test whether the degree to which E2 facilitated aggression (E2-CON) could be explained by the level of *ESR1* or *ESR2* expression, controlling for morph, using function *pcor.test* from the package *ppcor* (Kim, 2015; Kim & Yi, 2007) (v. 1.1). We also asked whether *ESR1* and *ESR2* expression were correlated with each other using a Pearson's correlation *cor.test* in base R.

Collection and processing of tissue for analysis of AI and methylation

Collection of free-living white-throated sparrows. Adults of both sexes and morphs were collected at Penobscot Experimental Forest near Argyle, ME during the peak of territorial behavior, after pair formation and territory establishment but prior to or early in the stage of incubation (Falls & Kopachena, 2020; Horton, Moore, et al., 2014). Before collecting the adults, we characterized their behavioral responses to territorial intrusion by conducting STIs. STIs were performed on two consecutive days at the same time each day. We presented either a TS or WS live male decoy in a counterbalanced order (Horton et al., 2012). During presentation of the decoy, conspecific song was played for ten min. Aggressive responses, including songs, were quantified for both the male and the female resident. At least 24 hr after the second STI, we returned to the site to collect both the male and the female. We used song playback to lure them quickly into a mist net. Average latency to capture was 6.1 ± 0.89 SE min after the onset of the song playback. There were no effects of sex ($F(1,18) = 0.167$, $P = 0.602$) or morph ($F(1,18) = 0.678$, $P = 0.686$) on time to capture, and no interaction between sex and morph ($F(1,18) = 0.138$, $P = 0.713$). Later in the breeding season, during the parental phase, we collected nestlings on post-hatch day seven, two days before natural fledging (Falls & Kopachena, 2020). All birds were sacrificed immediately after capture by isoflurane overdose. Brains were rapidly dissected from the skulls, frozen on dry ice and stored at -80 °C. Sex and morph for all birds were later confirmed by PCR (Griffiths et al., 1998; Thomas et al., 2008).

Microdissection. Our methods for quantifying *ESR1* expression in micropunched tissue have been described elsewhere (Grogan et al., 2019). Briefly, we cryosectioned

brains at 300 µm in the coronal plane, then used the Palkovits punch technique (Palkovits, 1973) to obtain 1 mm diameter samples from the regions of interest as previously described (Grogan et al., 2019; Zinzow-Kramer et al., 2015). TnA was sampled in each hemisphere in two consecutive sections for a total of four punches, which were pooled for nucleic acid extraction. For HYP, punches were centered on the midline such that they contained tissue from both hemispheres. One punch was made immediately ventral to the anterior commissure and included the caudal portion of the medial preoptic area, the paraventricular nucleus, and the anterior hypothalamus. A second punch was made ventral to the first and included the ventromedial hypothalamus. Both HYP punches were made in two consecutive sections for a total of four punches, which were pooled for nucleic acid extraction in the adult samples. Punches of the ventral and dorsal hypothalamus were kept separate for nestlings and expression was averaged during data analysis. For rostral rPOM, one punch was made underneath the septo-mesencephalic tract and above the supraoptic decussation.

RNA/DNA extraction. DNA and RNA were extracted using either the Qiagen Allprep RNA/DNA micro kit (Qiagen, Valencia, CA, USA) with modifications or the Qiagen miRNeasy micro kit (Qiagen, Valencia, CA, USA) with modifications as previously described (Zinzow-Kramer et al., 2015). The DNA was used for the bisulfite conversion, see below. The RNA was reverse transcribed into cDNA using the Transcriptor First Strand cDNA synthesis kit with random hexamer primers (Roche Diagnostics, Indianapolis, IN, USA). cDNA reactions were then diluted to 20 ng/µl for qPCR.

AI assay. To detect AI, primers (F: GCAGGATTTCACTCCCTGAA, R: TACCTGTTGGCTGTGATGATG) and allele-specific probes for the ZAL2 (CTGTCGCCCT) and ZAL2^{m} (CTGTCACCCT) alleles of *ESR1* were designed by Integrated DNA Technologies (Coralville, Iowa, USA) to target a SNP (NW_00508196.1:1801511) within *ESR1* Exon 1A following Chen et al. (Chen et al., 2008). cDNA from WS adults and nestlings was used (TS birds do not have the ZAL2^{m} allele). To increase the melting temperatures and thus specificity, the probes contained 4-6 locked nucleic acids. The probes were labeled on the 5' end with dye; 6-FAM was used for ZAL2 and 5Cy5 for ZAL2^{m}. All samples were run in triplicate in on a Roche LightCycler 480 Real-Time PCR System. In addition to experimental samples, each plate included the following controls: a negative cDNA reaction control with no template added, a negative cDNA reaction control with no RT enzyme added, positive controls of ZAL2/ZAL2 and ZAL2^{m}/ZAL2^{m} genomic DNA, and a positive control with a 5x dilution of WS gDNA to assess overall amplification efficiency. We also included a dilution curve from 1:8 to 8:1 of ZAL2: ZAL2^{m} genomic DNA to assess the specificity of the probe binding (Fig. A2). To correct for imperfect specificity of the probes, we also included >10 undiluted ZAL2/ZAL2^{m} genomic DNA samples on each plate. Each reaction contained approximately 5-25 ng of cDNA, depending on the brain region, 750 nM of forward and reverse primer, 6.0 ul of 2X Probes Master (Roche), and 200 nM of each probe. Cycling conditions were 95° C for 10 min, followed by 45 cycles of 95° C for 10 seconds, 60° C for 30 seconds, and 72° C for 1 second. We removed a maximum of one technical outlier from each triplicate (st. dev. > 0.2). Samples that produced hyper-

variable results or for which the reaction failed were not included in final analyses (final sample size for nestlings: HYP n = 26, TnA n = 27, rPOM n = 27; adults: HYP n = 18, TnA n = 18, rPOM n = 15). Each group comprised roughly equal numbers of males and females. We then used the Abs Quant/Fit Points method in the LightCycler 480 Software Version 1.5.0 to calculate relative expression from the Cp values, averaged across the three replicate reactions, then divided the value for ZAL2^{m} by the value for ZAL2. The primer efficiency was ~1.8 and the ratio of triplicate averages of each allele (cDNA) was normalized to the average of the ratios calculated from all of the gDNA samples (mean = 0.99, min = 0.95, max = 1.02) to correct for incomplete probe binding. We tested for AI within each region and age using one-sample t-tests comparing to a null ratio of 1 (Table A4). To determine whether the degree of AI varied by age or region, we analyzed the data in a two-way mixed ANOVA with region and age as factors, followed by Tukey's Honest Significant Difference (Table A5). Associations between AI and territorial responses were tested using Pearson's correlations.

Analysis of DNA methylation

bsDNA PCR and sequencing. We bisulfite-converted 200 ng of gDNA, extracted from the punches from TnA of the adults described above (see *Microdissection*), using the EZ DNA Methylation-Lightning Kit following the manufacturer's instructions (Zymo, Irvine, CA, USA). Thirteen amplicons containing shared and unshared CpG sites in the three CREs and exon 1A of *ESR1* were amplified using PCR with primers that do not fall on SNPs or CpGs (Table A9). Each 25 µl PCR included 0.5 µl JumpStart Taq DNA polymerase, 2.5 µl JumpStart buffer containing 40

mM $MgCl_2$, 5 nM of each primer, and 8 ng of bisulfite-converted DNA. The PCR protocol for each primer pair was optimized using a temperature and $MgCl_2$ gradient such that an additional 0-100 mM $MgCl_2$ was added to some reactions. Cycling conditions were 95°C for 60 seconds, then 40 cycles of 95°C for 30 seconds, 55°C for 30 seconds, and 70°C for 60 seconds, followed by a single final extension phase at 70°C for 5 min. Ten µl of each PCR product was visualized on a 1% agarose gel. Any PCRs that did not show a band were rerun, modifying the concentration of $MgCl_2$, until a band of the correct size was seen. All 13 amplicons for each sample were pooled and 5 µl of that pool was used for next-generation sequencing. Adapter-ligated libraries were constructed using the 16S Metagenomic Sequencing Library kit (Illumina; San Diego, USA) following the manufacturer's instructions. Samples were then run on the Agilent bioanalyzer to confirm successful indexing and quality of total DNA, then pooled for a single sequencing run (PE300) on the Illumina MiSeq at the Emory Integrated Genomics Core.

bsDNA filtering and mapping. We filtered reads at a Phred score of 30, then trimmed for low quality, Nextera adapter sequences, and indexes using Trim-galore! (v0.3.7) (Krueger, 2015). A bisulfite-converted reference genome was generated in Bismark (v0.18.1) (Krueger & Andrews, 2011) using the scaffold that contains *ESR1* (NW_005081596.1) from the genome of a TS bird (GCF_000385455.1) (Sun et al., 2020). This reference genome was N-masked at ZAL2/ZAL2^m fixed SNPs (Sun et al., 2018) in order to reduce mapping bias, and unshared ZAL2^m CpGs were added to the reference genome so that information on methylation state could be extracted for the highest possible number of CpGs. Bismark does not use CpGs to map reads, so this

modification did not introduce bias into our analysis. Reads were aligned using Bismark with bowtie2 (v2.3.5) (Langmead & Salzberg, 2012). Reads were then filtered for non-CpG methylation such that any read that included 3 C's in a row in non-CG positions was removed. Reads were then assigned to alleles on the basis of non-CpG fixed SNPs using SNPsplit (v0.3.4) (Krueger & Andrews, 2016). We then used Bismark (Krueger & Andrews, 2011) to extract methylation calls and generate bedGraphs that were imported into RStudio for further analysis.

Data analysis. CpGs were filtered for low coverage (<10x) and analyzed using a custom script in R. To arrive at an overall level of methylation for each of the two alleles for each bird, we averaged % methylation across all of the CpGs in that allele. When including unshared CpG sites, we treated that site on the other allele as 0% methylation. We then ran linear regressions with allele as a single factor with three levels, TS-ZAL2, WS-ZAL2, and WS-ZAL2^{m}, and with allele nested within bird as a random factor, using the *lme4* (v1.1-21) package (Bates et al., 2014) (Table A10). These results were summarized using the *car* (v3.0-3) package (Fox & Weisberg, 2011) and post-hoc tests (estimated marginal means contrasts controlling for individual) were conducted using the *emmeans* (v1.4.3.01) (Russell, 2018) package. We then created Pearson correlation matrices to identify clusters of significantly correlated CpGs within each allele. We averaged % methylation across the CpGs within each cluster (six clusters on ZAL2, five on ZAL2^{m}) following established protocols (Rubenstein et al., 2016; Siller & Rubenstein, 2019). We then used Pearson correlations to calculate the extent to which the % methylation of each cluster predicted allele-specific expression in our RNA-seq data. For males (n = 8 TS, 10 WS), we used normalized read counts from previously published

RNA-seq data (Sun et al., 2018; Zinzow-Kramer et al., 2015). For females (n = 6 TS, 6 WS), we used normalized read counts from new RNA-seq data (see next section).

RNA-seq library preparation, sequencing, and data analysis. Library preparation and sequencing of mRNA from six TS females and six WS females were performed by the Duke Center for Genomic and Computational Biology Sequencing and Genomic Technologies Core in Durham, NC. After assessing the RNA quality using Qubit and Agilent Tapestation (Agilent Technologies, Santa Clara, CA, USA), RNA-seq libraries were constructed using a Kapa Stranded mRNA-Seq Kit (Kapa Biosystems, Boston, MA, USA) following the manufacturer's instructions. The samples were then pooled and sequenced on an Illumina HiSeq 4000 in pools of 8-10 samples per lane in 150 paired-end reactions. We obtained 20-45 million read pairs per sample. RNA-seq files were trimmed using Trim-galore! (v0.4.5) (Krueger, 2015) retaining only pairs of sequences for which all bases had an average Phred score of 30. Again to control for mapping bias towards the reference (ZAL2/ZAL2) genome, we mapped all reads to the above-mentioned N-masked genome (Sun et al., 2018). Reads were mapped with STAR (v2.5.2b) (Dobin et al., 2013) using the 2-pass mode, and only uniquely mapped reads were retained for differential expression analysis. To obtain read counts of *ESR1* at the allele level, reads were assigned to ZAL2 or ZAL2^{m} using SNPsplit (v0.3.3) (Krueger & Andrews, 2016), counted by htseq-count (v0.11.1) (Anders, Pyl, & Huber, 2015), and then normalized and analyzed using DESeq2 (v1.24.0) (Love et al., 2014).

Analysis of *cis*-regulatory variation in *ESR1*

Analysis of transcription factor binding sites. We examined the CREs in *ESR1*

to identify transcription factor binding sites that are disrupted by ZAL2/2^{m}. To predict differential transcription factor binding between the two alleles, we used sTRAP, a transcription factor affinity predictor tool for SNPs (Manke et al., 2010; Okhovat et al., 2017). We submitted 42 ZAL2 and ZAL2^{m} sequences of 120 bp each, centered at each fixed sequence difference (41 SNPs and one indel), to sTRAP (Manke et al., 2010). We selected "transfact.12.1 metazoans" with the "chordate_conserved_elements" background model. sTRAP computed the affinity of transcription factors for each allele, then ranked the difference in p-values between the alleles ($\log_{10}$(ZAL2 p-value/ZAL2^{m} p-value)). We corrected for multiple comparisons using Benjamini-Hochberg corrections. Position weight matrices with significant ($P < 0.05$) affinity for at least one allele and a p-value ratio >1.5 were considered by sTRAP to be differential binding sites. We entered the list of predicted differential sites into TRANSFAC version 2019.2 to create a comprehensive list of associated transcription factors predicted to bind with greater affinity to one allele than the other. Finally, we cross-referenced the list of factors predicted to bind differentially to the two alleles with the list of factors that are expressed in TnA (Zinzow-Kramer et al., 2015).

Luciferase assays. A 2 kb sequence upstream of each transcription start site of *ESR1* was amplified by PCR using gDNA from a WS (ZAL2/ZAL2^{m}) bird, then cloned upstream of firefly luciferase into the pGL3-control vector at the KpnI and MluI restriction sites (Fig. A3; Table A9). Clones containing the ZAL2 or ZAL2^{m} alleles were identified, on the basis of known fixed differences, via Sanger sequencing by Genscript (Piscataway, NJ, USA). Luciferase reporter assays were performed in three different cell types: HeLa, HEK-293, and DT40 cells. HEK-293 cells were cultured in DMEM

supplemented with 10% FBS (Atlanta Biologicals). HeLa cells were cultured in MEMα supplemented with 10% FBS. DT40 cells were cultured in DMEM with 10% FBS and 5% chicken serum and supplemented daily with 0.05 mM 2-mercaptoethanol following ATCC guidelines (https://www.atcc.org/products/all/CRL-2111.aspx). Two hundred ng of each construct was co-transfected into cells, along with 10 ng of constitutively expressed Renilla luciferase, using FuGene HD (Promega) in OptiMEM. Data collection was completed separately for each cell type as follows: 24 hr after transfection, the activities of firefly and Renilla luciferase were read three times using the Dual-Glo assay system (Promega) on a Biotek Synergy plate reader. These three readings were then averaged for firefly luciferase as well as for Renilla luciferase. The average reading for firefly luciferase was normalized to that of Renilla luciferase for each well. This normalized value was then averaged across five replicates. The resulting value for the $ZAL2^m$ allele was then normalized to the value for the ZAL2 allele, meaning that the $ZAL2^m$ data were expressed relative to a value of 1 for the ZAL2 allele. Experiments were replicated three times for the HeLa and HEK cells and six times for the DT40 cells; results were averaged across experiments. Effects of CRE (A, B, or C), allele, and the interaction between CRE and allele were assessed using a 2-way ANOVA. When significant effects or interactions were found, we used Student's pairwise t-tests to test for the effect of allele within each CRE.

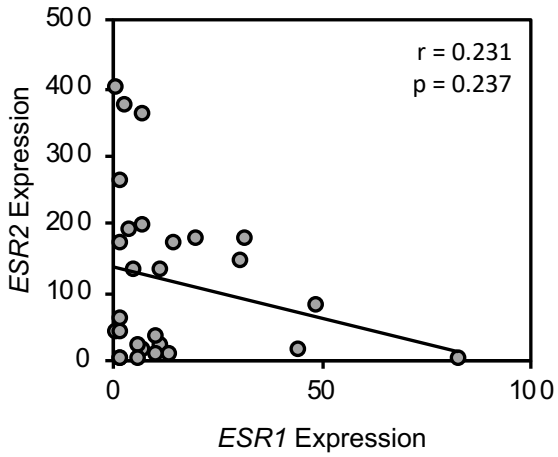

Figure A1. The relationship between *ESR1* and *ESR2* expression, as measured by qPCR, in TnA of birds in the knockdown experiment (see Fig. 2). Only birds receiving scrambled control oligonucleotides or for which the antisense infusions missed TnA are included here (n = 20).

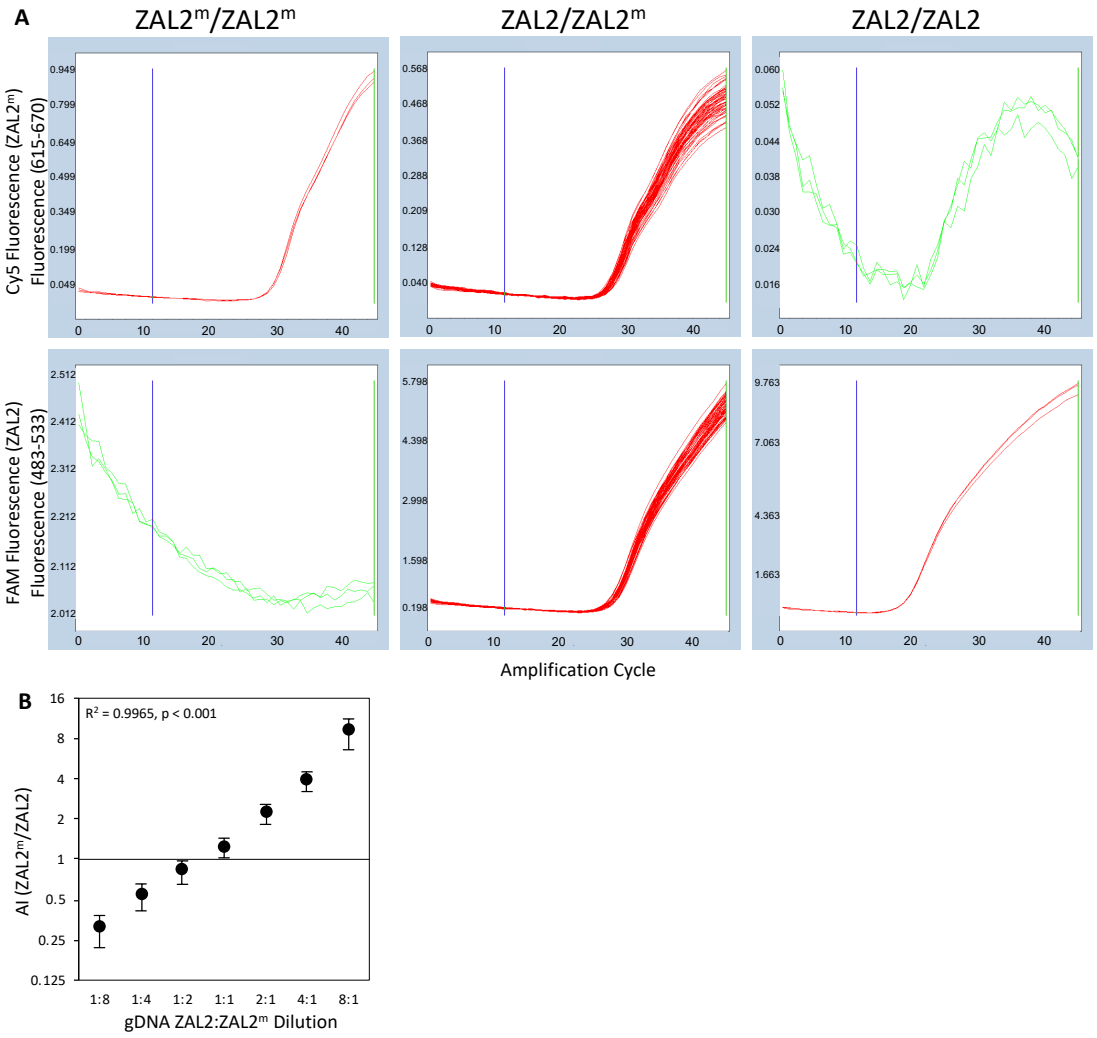

Figure A2. Validation of the AI assay. (A) Allele-specific qPCR amplification curves for ZAL2 and ZAL2^m genomic DNA demonstrate that the probes selectively amplify the targeted allele (ZAL2^m/ZAL2^m, n = 1; ZAL2/ZAL2^m n = 12, ZAL2/ZAL2 n = 1; run in triplicate). Note the difference in the Y-axis scale in the top right and bottom left (green) – no amplification curves were observed in those cases. (B) An example of an AI standard curve of dilutions from 1:8 to 8:1 of ZAL2: ZAL2^m genomic DNA. Mean + SEM, n = 3 per dilution (y = 0.1644e0.5403).

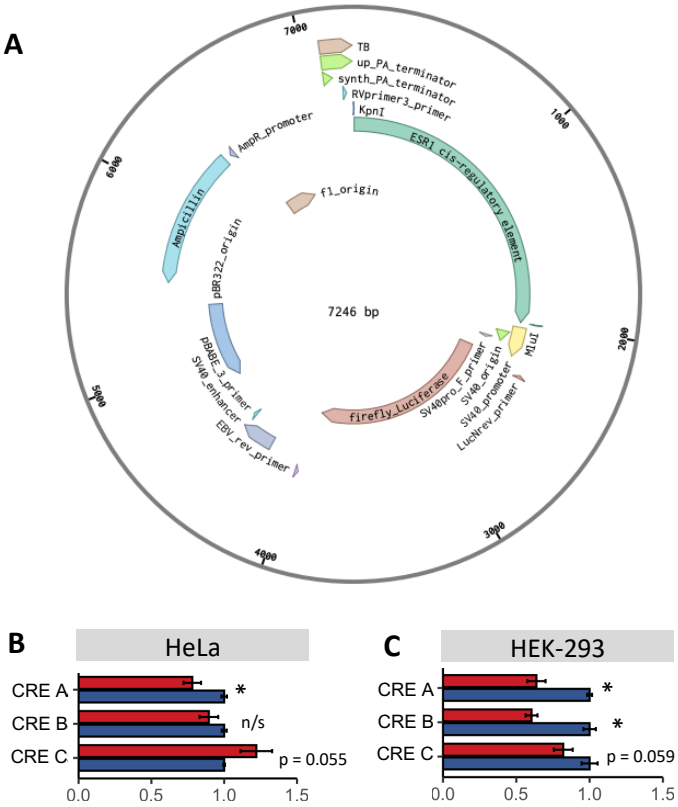

Figure A3. Design and results of luciferase assays. (A) The *ESR1 cis*-regulatory elements (CREs) were cloned into the pGL3-control vector (Genbank E1741) at KpnI and MluI cut sites upstream of the firefly luciferase gene. *Cis*-regulatory variation in *ESR1* affected luciferase activity *in vitro* in HeLa (B) and HEK-293 (C) cells. The activity, in RLU, of the ZAL2^{m}-luciferase (LUC) (red) and ZAL2-LUC (blue) constructs is shown normalized to the activity of the ZAL2-LUC construct. n =3, * $P <$ 0.05; see Table A7 for all p values. The direction of the effect of allele was opposite in HEK cells, compared with HeLa cells (B) and DT40 cells (Fig. 4). This result is consistent with variation in local availability of transcription factors in lines of cultured cells (Geiger, Wehner, Schaab, Cox, & Mann, 2012). The local complement of transcription factors in each cell line is expected to interact differently with the ZAL2 and ZAL2^{m} alleles (see Fig. 4), which could change the direction of the overall effect of allele.

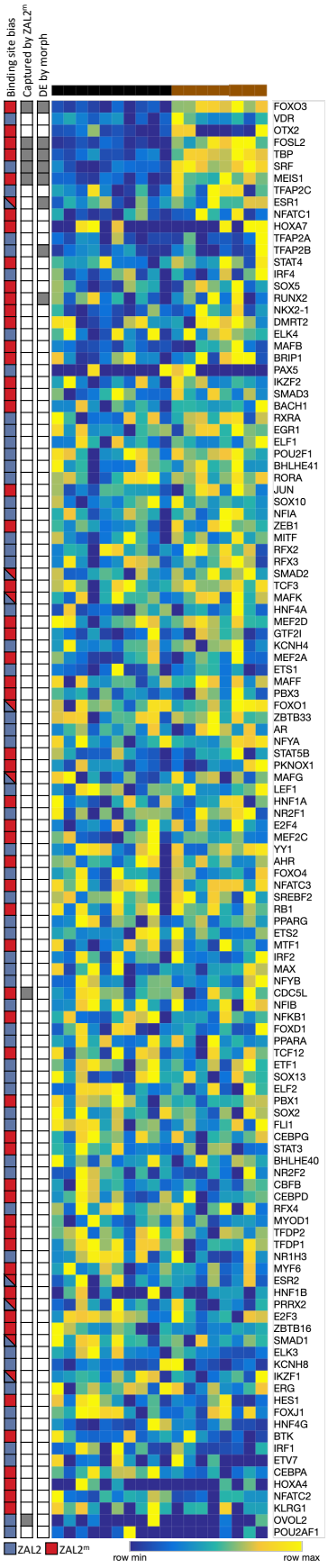

Figure A4. Expression of 120 TFs with binding sites disrupted by ZAL2/ZAL2^{m} fixed SNPs in the *ESR1* *cis*-regulatory elements (see Fig. 4). Gene expression is shown from RNA-seq data normalized using "estimateSizeFactors" in DESeq2 in WS males (black, n =10) and TS males (brown, n = 8) (Love, Huber, & Anders, 2014). RNA was extracted from TnA. Each row represents a gene and each column represents an individual. Genes are ordered according to fold difference between WS and TS birds. TFs that were differentially expressed by morph (Benjamini-Hochberg correction at FDR = 0.1) or captured by ZAL2^{m} are marked with a light grey box to the left. On the far left, TFs are color-coded red or blue according to allelic bias, in other words according to which allele contains one or more binding sites predicted to have higher affinity for that particular TF than the corresponding site(s) on the other allele. Eight TFs are coded as both blue and red because multiple binding sites for those TFs were disrupted; for half of those sites, the ZAL2 allele is predicted to have higher affinity for transcription factors whereas for the rest, ZAL2^{m} is predicted to have higher affinity. Overall, these results show that transcription factors with impacted binding sites were neither overrepresented on ZAL2^{m} nor enriched for differential expression by morph.

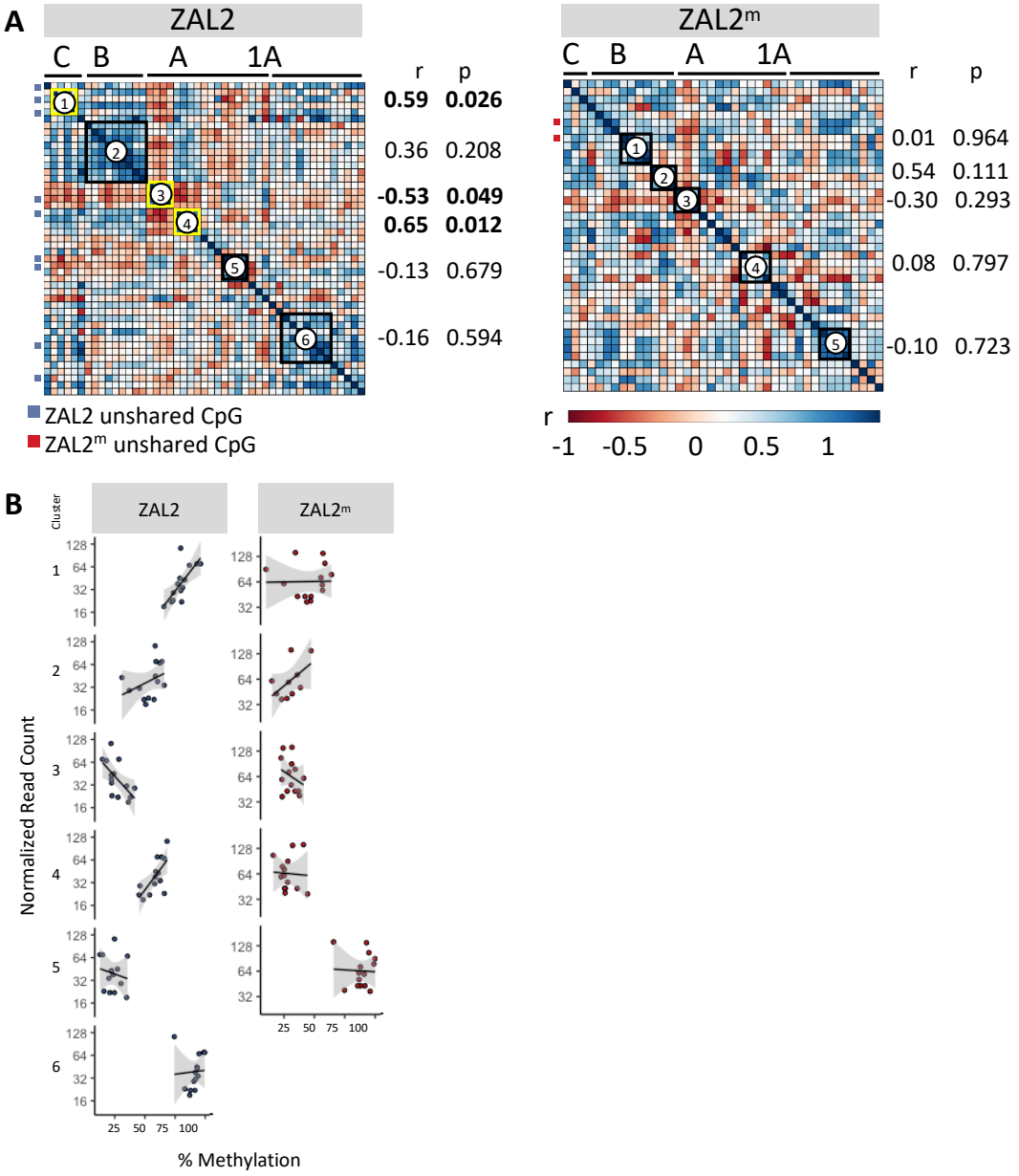

Figure A5. Allele-specific methylation predicts allele-specific expression. (A) Correlation matrices using data from WS birds are shown (see also Fig. 4). Similarly methylated clusters of sites are enclosed in boxes and numbered (see Fig. 4E in the main text for the figure with clusters unobscured). The clusters were used to test for associations between allele-specific methylation and allele-specific expression in the same animals. Clusters that significantly predicted allele-specific expression are outlined in yellow, clusters that did not are outlined in black. Unshared sites are marked by boxes to the left of each matrix. (B) Scatterplots show the relationships between allele-specific methylation and allele-specific expression (from RNA-seq data; see Methods) for the clusters shown in (A). n = 15, * $P < 0.05$.

Table A1. Effects of *ESR1* knockdown (oligo type) and morph on *ESR1* expression in nucleus taeniae of the amygdala. *P*-values are shown for post-hoc* tests (Tukey's Honest Significant Difference).

	Effect of Oligo Type within Morph		Effect of Morph within Oligo Type
Morph	*ESR1*-KD vs. Scrambled (*P*-values)	Oligo Type	WS vs. TS (*P*-values)
TS	0.994	*ESR1*-KD	0.947
WS	0.048	Scrambled	0.011

* An ANOVA showed a main effect of oligo type ($F(1,18) = 4.46$, $P = 0.049$), a main effect of morph ($F(1,18) = 8.82$; $P = 0.008$) and an interaction between oligo type and morph ($F(1,18) = 4.84$; $P = 0.041$).

Table A2. Effects of estradiol treatment and morph on aggression. $\chi 2$ and *P*-values are shown for the GLMs accompanying Fig. 2C,F. Numerator degrees of freedom for all below are = 1, denominator d.f. are in parenthesis next to $\chi 2$. AIC values and results from log-likelihood ratio tests comparing the models with or without the interaction term are reported for each GLM. "Opponent" refers to the subordinate conspecific presented to the focal animal during the behavioral trial.

		Attacks		Time Spent Near the Opponent (s)	
Birds receiving scrambled oligos		$\chi 2$ (10)	*P*	$\chi 2$ (10)	*P*
	Morph	0.34	0.559	0.02	0.886
	Treatment	0.07	0.790	0.37	0.542
	Minute	5.74	0.017	22.69	< 0.001
	Morph × Treatment	14.72	< 0.001	8.00	0.005
		AIC = 1469.19 with interaction; AIC = 1484.48 without interaction. $\chi 2$ (1) = 17.287, P < 0.001		*AIC = 2338.72 with interaction; AIC = 2342.23 without interaction. $\chi 2$ (1) = 5.510, P = 0.019*	
Birds receiving *ESR1* knockdown		$\chi 2$ (8)	*P*	$\chi 2$ (8)	*P*
	Morph	0.00	0.996	6.14	0.013
	Treatment	0.56	0.456	11.24	< 0.001
	Minute	0.44	0.509	14.02	< 0.001
	Morph × Treatment	0.14	0.712	0.49	0.483
		AIC = 1103.81 with interaction; AIC = 1102.53 without interaction. $\chi 2$ (1) = 0.722, P = 0.395		*AIC = 2192.80 with interaction; AIC = 2192.11 without interaction. $\chi 2$ (1) = 1.311, P = 0.252*	

Table A2 (continued)

		Attacks		Time Spent Near the Opponent (s)	
WS birds		$\chi 2$ (9)	*P*	$\chi 2$ (9)	*P*
	Antisense	24.41	< 0.001	9.64	0.002
	Treatment	5.03	0.025	0.24	0.627
	Minute	13.32	< 0.001	20.21	< 0.001
	Antisense × Treatment	4.43	0.035	9.53	0.002
		AIC = 1356.22 with interaction; AIC = 1359.41 without interaction. $\chi 2$ (1) = 5.192, P = 0.023		*AIC = 2333.20 with interaction; AIC = 2336.71 without interaction. $\chi 2$ (1) = 5.509, P = 0.019*	
TS birds		$\chi 2$ (9)	*p*	$\chi 2$ (9)	*p*
	Antisense	15.53	< 0.001	0.04	0.837
	Treatment	8.04	0.005	9.77	0.002
	Minute	0.00	0.976	16.19	< 0.001
	Antisense × Treatment	4.46	0.035	1.21	0.271
		AIC = 1274.19 with interaction; AIC = 1276.71 without interaction. $\chi 2$ (1) = 4.517, P = 0.034		*AIC = 2197.36 with interaction; AIC = 2196.60 without interaction. $\chi 2$ (1) = 1.236, P = 0.266*	

Table A3. Effects of E2 administration on aggression within experimental group (morph/oligo type). χ^2 and *P*-values are shown for the GLMs for Fig. 2C,F.

		Attacks		Time Spent Near the Opponent (s)	
TS Scrambled		$\chi 2$ (5)	*P*	$\chi 2$ (5)	*P*
	Treatment	7.48	0.006	9.81	0.002
	Minute	0.00	0.977	16.24	< 0.001
WS Scrambled		$\chi 2$ (5)		$\chi 2$ (5)	
	Treatment	6.58	0.010	6.96	0.008
	Minute	8.35	0.004	16.59	< 0.001
TS *ESR1*-KD		$\chi 2$ (4)		$\chi 2$ (4)	
	Treatment	0.57	0.451	8.20	0.004
	Minute	1.17	0.279	8.55	0.003
WS *ESR1*-KD		$\chi 2$ (4)		$\chi 2$ (4)	
	Treatment	0.07	0.796	3.24	0.072
	Minute	6.29	0.012	5.44	0.020

Table A4. Allelic imbalance in *ESR1* expression in HYP, rPOM, and TnA. See Fig. 3. *t* and *P*-values for one-sample t-tests are shown.

	Adults		Nestlings	
Region	*t* (d.f.)	*P*	*t* (d.f.)	*P*
HYP	-10.903 (15)	< 0.001	-4.778 (25)	< 0.001
POM	-8.071 (13)	< 0.001	-12.569 (26)	< 0.001
TnA	4.739 (15)	< 0.001	2.616 (25)	0.015

Table A5. Effects of region and age on the degree of allelic imbalance in *ESR1* expression in HYP, rPOM, and TnA. *P*-values are shown for post-hoc* tests (Tukey's Honest Significant Difference). See Fig. 3.

	Region effects within Adults (*P*-value)			Region effects within Nestlings (*P*-value)			Age effects within Region (*P*-value)
Region	HYP	POM	TnA	HYP	POM	TnA	
HYP	-	0.999	< 0.001	-	0.997	0.059	0.988
POM	0.999	-	< 0.001	0.997	-	0.019	0.999
TnA	< 0.001	< 0.001	-	0.059	0.019	-	< 0.001

* An ANOVA showed a main effect of region ($F(2,250) = 82.86$, $P < 0.001$), a main effect of age ($F(1,250) = 13.54$; $P < 0.001$) and an interaction between region and age ($F(2,250) = 12.90$; $P < 0.001$).

Table A6. Fixed SNPs and indels in the *ESR1* CREs.

Accession	Position	ZAL2/ZAL2^{m}	CRE	Dist. from TSS
NW_005081596.1	1725878	G/C	C	-1952
NW_005081596.1	1725935	C/T	C	-1895
NW_005081596.1	1726061	G/C	C	-1769
NW_005081596.1	1726101	C/G	C	-1729
NW_005081596.1	1726110	C/T	C	-1720
NW_005081596.1	1726277	T/C	C	-1553
NW_005081596.1	1726287	A/G	C	-1543
NW_005081596.1	1726299	C/T	C	-1531
NW_005081596.1	1726315	G/C	C	-1515
NW_005081596.1	1726484	G/T	C	-1346
NW_005081596.1	1727022	T/A	C	-808
NW_005081596.1	1727091	C/G	C	-739
NW_005081596.1	1727273	T/C	C	-557
NW_005081596.1	1727539	C/T	C	-291
NW_005081596.1	1747958	T/A	B	-1456
NW_005081596.1	1747993	A/G	B	-1421
NW_005081596.1	1748584	T/C	B	-830
NW_005081596.1	1748651	T/G	B	-763
NW_005081596.1	1748701	G/A	B	-713
NW_005081596.1	1748949	A/G	B	-465
NW_005081596.1	1749043	A/G	B	-371
NW_005081596.1	1749073	TA/T	B	-341
NW_005081596.1	1749079	A/T	B	-335
NW_005081596.1	1749359	C/G	B	-55
NW_005081596.1	1749401	C/T	B	-13
NW_005081596.1	1799245	C/A	A	-1857
NW_005081596.1	1799456	C/A	A	-1646
NW_005081596.1	1799677	A/T	A	-1425
NW_005081596.1	1799821	T/A	A	-1281
NW_005081596.1	1800307	G/A	A	-795
NW_005081596.1	1800338	T/C	A	-764
NW_005081596.1	1800343	A/G	A	-759
NW_005081596.1	1800344	A/C	A	-758
NW_005081596.1	1800347	C/A	A	-755
NW_005081596.1	1800648	T/C	A	-454
NW_005081596.1	1800745	A/G	A	-357
NW_005081596.1	1800769	G/A	A	-333
NW_005081596.1	1800798	G/A	A	-304
NW_005081596.1	1800878	C/T	A	-224

Table A7. Effects of CRE and allele on luciferase activity in three cell types (see Figs. 4B and A3). F (d.f.) and *p*-values are shown for a 2-way ANOVA. *P*-values are shown for post-hoc comparisons (Student's pairwise t-test) within CRE.

Main effects and interactions

	CRE		Allele		CRE x Allele	
	F	*P*	*F*	*P*	*F*	*P*
DT40	1.67 (2,128)	0.193	22.92 (1,128)	< 0.001	1.74 (2,128)	0.18
HEK-293	2.76 (2,30)	0.079	59.76 (2,30)	< 0.001	2.76 (2,30)	0.079
HeLa	8.14 (2,101)	< 0.001	1.13 (1,101)	0.29	7.1 (2,101)	0.001

Effects of allele within each CRE

Cell type	CRE A (*P*)	CRE B (*P*)	CRE C (*P*)
DT40	0.019	0.016	0.004
HEK-293	0.002	< 0.001	0.059
HeLa	0.002	0.129	0.058

Table A8. CpGs in the *ESR1* CREs and exon 1A in accession NW_005081596.1.

Position	ZAL2/ZAL2^{m}	CRE	Annotation	Dist. from TSS
1726299	CG/TG	C	unshared_CpG_ZAL2	-1531
1726431	CG/CG	C	shared_CpG	-1399
1726483	CG/CT	C	unshared_CpG_ZAL2	-1347
1726858	CG/CG	C	shared_CpG	-972
1727091	CG/GG	C	unshared_CpG_ZAL2	-739
1727328	CG/CG	C	shared_CpG	-502
1748236	CG/CG	B	shared_CpG	-1178
1748569	CG/CG	B	shared_CpG	-845
1748650	CT/CG	B	unshared_CpG_ZAL2^{m}	-764
1748695	CG/CG	B	shared_CpG	-719
1748948	CA/CG	B	unshared_CpG_ZAL2^{m}	-466
1749027	CG/CG	B	shared_CpG	-387
1749148	CG/CG	B	shared_CpG	-266
1749156	CG/CG	B	shared_CpG	-258
1749208	CG/CG	B	shared_CpG	-206
1749356	CG/CG	B	shared_CpG	-58
1749414	CG/CG	B	shared_CpG	0
1799180	CG/CG	A	shared_CpG	-1923
1799225	CG/CG	A	shared_CpG	-1878
1799245	CG/AG	A	unshared_CpG_ZAL2	-1857
1799324	CG/CG	A	shared_CpG	-1779
1799456	CG/AG	A	unshared_CpG_ZAL2	-1646
1799495	CG/CG	A	shared_CpG	-1608
1799534	CG/CG	A	shared_CpG	-1569
1799899	CG/CG	A	shared_CpG	-1204
1800143	CG/CG	A	shared_CpG	-960
1800387	CG/CG	A	shared_CpG	-716
1800484	CG/CG	A	shared_CpG	-619
1800768	CG/CA	A	unshared_CpG_ZAL2	-334
1800797	CG/CA	A	unshared_CpG_ZAL2	-305
1800856	CG/CG	A	shared_CpG	-247
1800859	CG/CG	A	shared_CpG	-244
1800884	CG/CG	A	shared_CpG	-219
1800978	CG/CG	A	shared_CpG	-125
1801023	CG/CG	A	shared_CpG	-80
1801121	CG/CG	Exon1A	shared_CpG	18
1801127	CG/CG	Exon1A	shared_CpG	24
1801288	CG/CG	Exon1A	shared_CpG	185

Table A8 (continued)

Position	ZAL2/ZAL2^{m}	CRE	Annotation	Dist. from TSS
1801295	CG/CG	Exon1A	shared_CpG	192
1801304	CG/CG	Exon1A	shared_CpG	201
1801369	CG/CG	Exon1A	shared_CpG	266
1801376	CG/CA	Exon1A	unshared_CpG_ZAL2	274
1801393	CG/CG	Exon1A	shared_CpG	290
1801468	CG/CG	Exon1A	shared_CpG	365
1801477	CG/CG	Exon1A	shared_CpG	374
1801495	CG/CG	Exon1A	shared_CpG	392
1801509	CG/CA	Exon1A	unshared_CpG_ZAL2	406
1801559	CG/CG	Exon1A	shared_CpG	456
1801574	CG/CG	Exon1A	shared_CpG	471

Table A9. Primers used to make CRE constructs for luciferase assays and amplicons for next-generation bisulfite sequencing. Primers for luciferase assays included restriction cut sites for KpnI (F: GGTACC) or MluI (R: ACGCGT) on the 5' end of the primer. The bisulfite primers included Nextera transposase adapters on the 5' end of the primer (F: TCGTCGGCAGCGTCAGATGTGTATAAGAGACAG; R: GTCTCGTGGGCTCGGAGATGTGTATAAGAGACAG).

Luciferase assay	
Primer Name	Primer Sequence (5' → 3')
ESR1A_F	TGCAGCTTAATAAGGGATGATGC
ESR1A_R	ACCAGAACCTATTCTGAGGCT
ESR1B_F	GGTAAAGCAGGCCACTGTTAC
ESR1B_R	AGCAGGCTGTTGCCATTC
ESR1C_F	GCCATATAAGCAAGAGGGC
ESR1C_R	CTCATTGGCAGTCACCAAG

Bisulfite amplicon sequencing	
ESR1A_F_bs_89	ATGTGTTAGGGTGATTGGTTTAAAT
ESR1A_R_bs_574	CAATACTTTCAAAACTCCTACTAAAATAAC
ESR1A_F_bs_96	GGGTGATTGGTTTAAATTTGTAGTT
ESR1A_R_bs_527	CAAAAATATTCTAAAACAATATATATTTTT
ESR1A_F_bs_737	GTTGGAGTTTATATATTAATGTATTTAGGG
ESR1A_R_bs_1179	ATCATTTACATTTTATCAAAATTAAAAAAT
ESR1A_F_bs_1269	AGTGTTTTAGTAATTGTAAGTTGTTGTTGT
ESR1A_R_bs_1579	CCTCCTATTTAATTCATTTTCATATTTACT
ESR1A_F_bs_1656	TTTGGTTGGATTTAGTGTTTTTTTT
ESR1A_R_bs_2116	CAAAAAACATATCTACTTTTACTATCAACA
ESR1B_F_bs_1828	TTTTAATTTATTTGTTTAGTTTTTGATT
ESR1B_R_bs_2190	CTAACTACTATAATAAATCACCAAATCTTC
ESR1B_F_bs_1021	AAAATTTTTGTTGGGGTATTTTGTA
ESR1B_R_bs_1370	AACTAACTCACAAAACCTTCTAAATAAACA
ESR1B_F_bs_1562	TTGTTTTGGAAATAAGGTAATTTTGATA
ESR1B_R_bs_2001	ACTATAAACACATCTCAAAAATTACTTTCA
ESR1B_F_bs_2055	AAATTATTGGAAATTTTAGTTTTAAGA
ESR1B_R_bs_2494	AACAAACTATTACCATTCCCTCTAC
ESR1C_R_bs_424	GAAGGAAGGGTTTGTTTATTATGATT
ESR1C_F_bs_837	TCCATCTCCTCAAAATAATATCTAATATCT
ESR1C_R_bs_915	AGGAGGAATAGATTAATGTAAGGAATTAAA
ESR1C_F_bs_1313	TCAACACCTACATTACAAAATATAAATAAA
ESR1C_F_bs_1226	AAGTTAGTAGATAGTAGAGAAGTTAGAAGA
ESR1C_R_bs_1622	AAATAATTTAACACAATTTCTTTCCC
ESR1E1_F_bs_129	AAGGTATTGAATTGGAGATATTGAGTAG
ESR1E1_R_bs_499	AACTAAAAAAACAACTTCCCTCATC

Table A10. Effects of allele on percent methylation of *ESR1* CREs and exon 1A. (see Fig. 4). DNA was extracted from TnA. *P*-values are shown for post-hoc* comparisons (estimated marginal means contrasts) controlling for individual.

Effects of Allele	All sites (*P*-value)	Shared Sites Only (*P*-value)
ZAL2 (TS) vs. ZAL2 (WS)	0.933	0.903
ZAL2 (WS) vs. ZAL2^{m} (WS)	< 0.001	0.984
ZAL2 (TS) vs. ZAL2^{m} (WS)	< 0.001	0.961

* A linear mixed model with fixed effect of allele and random effect of allele nested within bird showed a main effect of allele ($F(2,96) = 21.387$, $P < 0.001$) when considering all sites. The same model with the shared sites only did not yield a significant effect of allele ($F(2,96) = 0.322$, $P = 0.727$).